Journal of Structural Geology 33 (2011) 203–219

Contents lists available at ScienceDirect

Journal of Structural Geology

journal homepage: www.elsevier.com/locate/jsg

A critique of vorticity analysis using rigid clasts

Changcheng Li*, Dazhi Jiang

Department of Earth Sciences, University of Western Ontario, London, Ontario, Canada N6A 5B7

ARTICLE INFO

Article history:
Received 15 January 2010
Received in revised form
24 June 2010
Accepted 2 September 2010
Available online 15 September 2010

Keywords:
Monoclinic flow
Rigid clast
Shear zone
Transpression
Vorticity number
Vorticity analysis

ABSTRACT

Estimating the kinematic vorticity numbers from rock fabrics presents many problems. In this paper we use numerical modeling to investigate the reliability of those widely-used vorticity analysis methods using rigid clasts. We use very simple flows (steady state, homogeneous, and having monoclinic symmetry) to represent plane-straining zones and transpressional zones and assume that the rotation of rigid clasts perfectly obeys the theory of Jeffery (1922, Proceedings of the Royal Society of London A102, 161–179). These are assumptions made in current vorticity analysis using rigid clasts. Even with these simple assumptions, our modeling shows that the current methods have intrinsic uncertainties so large that it is pointless to use the estimated vorticity numbers to constrain shear zone boundary conditions and kinematics. It is perfectly consistent with numerical modeling results if the currently reported vorticity numbers estimated from rigid clasts (in the range of 0.50–0.85) are all interpreted as being from natural shear zones with close-to-simple-shearing flows. The large uncertainties arise because the motion of rigid clasts is intrinsically a three dimensional problem.

1. Introduction

Ductile shear zones are common features in Earth's crust and mantle (e.g., Ramsay and Graham, 1970; Tchalenko, 1970; Mitra, 1978; Ramsay, 1980; Pili et al., 1997; Savage, 1999 and references therein; Regenauer-Lieb and Yuen, 2003; Vauchez and Tommasi, 2003; Williams and Jiang, 2005). Understanding the kinematics of such zones is important for elucidating the tectonic evolution of an area on a regional or larger scale. Many people have attempted to estimate the (kinematic) vorticity number of ductile shear zones from fabrics, although as pointed out by Tikoff and Fossen (1995), the vorticity number alone cannot completely characterize the kinematics of a shear zone unless it is an isochoric plane-straining[1] zone. To completely characterize the kinematics of a general monoclinic shear zone requires three independent parameters (Passchier, 1997, 1998). To completely characterize the kinematics of a triclinic shear zone requires four independent parameters (Jiang and Williams, 1998).

Many fabric types have been used for vorticity analysis, including deformed dykes or veins (e.g., Passchier and Urai, 1988; Wallis, 1992; Short and Johnson, 2006; Kuiper and Jiang, 2010), quartz and calcite lattice preferred orientations (LPO) (e.g., Wenk et al., 1987; Vissers, 1989; Ratschbacher et al., 1991; Wallis, 1992, 1995), tension gashes (e.g., Fossen and Tikoff, 1993; Grasemann et al., 1999), and rigid clasts (e.g., Passchier, 1987; Wallis et al., 1993; Simpson and De Paor, 1997). Among these, rigid clasts in mylonites are most commonly used (e.g., Klepeis et al., 1999; Xypolias and Koukouvelas, 2001; Bailey and Eyster, 2003; Law et al., 2004; Jessup et al., 2006; Marques et al., 2007; Wang et al., 2007; Kurz and Northrup, 2008; Sarkarinejad and Azizi, 2008; Sarkarinejad et al., 2009; Zhang et al., 2009; Langille et al., 2010; Thigpen et al., 2010). With the assumption (mostly implicit) that the deformation is plane straining, the estimated vorticity numbers have been extrapolated to infer large scale tectonic boundary conditions of some major shear zones in mountain belts (e.g., Wallis et al., 1993; Wallis, 1995; Grasemann et al., 1999; Xypolias and Koukouvelas, 2001; Law et al., 2004; Frassi et al., 2009). For instance, Grasemann et al. (1999) used their estimated vorticity numbers (0.57–0.71) from tension gashes and quartz LPO in the Main Central Thrust Zone to suggest an extrusion model after Grujic et al. (1996) for the exhumation of the crustal wedge bounded by the South Tibetan detachment zone and the Main Central Thrust Zone in NW Himalaya. Law et al. (2004) further supported this conclusion with their own estimated vorticity numbers (0.67–0.98) mainly from rigid clasts at the top of the

* Corresponding author. Tel.: +1 519 636 6068; fax: +1 519 661 3198.
E-mail addresses: cli246@uwo.ca (C. Li), djiang3@uwo.ca (D. Jiang).

[1] In this paper, to differentiate flow fields from finite deformation states, we use terms like simple shearing, pure shearing, and plane straining, following Means (1990), as opposed to simple shear, pure shear, and plane strain. Some authors have used terms like progressive simple shear (or simple shear progressive deformation), progressive pure shear (or pure shear progressive deformation) for the same purpose (e.g., Hobbs et al., 1976; Passchier, 1990; Jiang, 2010).

0191-8141/$ – see front matter © 2010 Elsevier Ltd. All rights reserved.
doi:10.1016/j.jsg.2010.09.001

crustal wedge. Xypolias and Koukouvelas (2001) carried out vorticity analysis using rigid clasts and quartz LPO throughout the Chelmos Shear Zone in Greece and used the results to support an extrusion model for the zone (Xypolias and Doutsos, 2000). In all these extrapolations, plane-straining deformation was assumed implicitly.

Many authors have pointed out that the vorticity analysis is based on some strict assumptions that are hard to justify for natural deformation. First, most fabrics result from accumulated deformation. In order for vorticity analysis to make sense, one must assume that the vorticity number has been constant during the development of the fabric. This essentially requires that the flow be steady state, which is hard to justify because deformation in natural shear zones is generally heterogeneous which is generally non-steady (Jiang, 1994; Jiang and White, 1995; Jiang and Williams, 1999). Regional to crustal scale shear zones commonly have a transposition foliation parallel to the shear zone boundaries (e.g., Williams and Jiang, 2005). It can be demonstrated that the transposition process is associated with highly non-steady flow in rheologically different lithological domains (e.g., Jiang, 1999, 2010). There is some belief that the vorticity number obtained from rocks might represent some "mean" or "average" vorticity number in the event that the flow has been non-steady. However, there is no theoretical or experimental basis for this belief. Second, the most widely-used vorticity analysis methods are based on rigid clasts and assume that they behave according to Jeffery's theory (Jeffery, 1922) for rigid inclusion motion in Newtonian viscous flows. However, rocks are likely non-Newtonian (Carter, 1975, 1976; Tullis, 1979; Kirby, 1983; Gleason and Tullis, 1995). Furthermore, many recent works have shown that clasts in rocks may not behave according to Jeffery's theory because of interface slip between clasts and the surrounding material (Ildefonse and Mancktelow, 1993; Bjørnerud and Zhang, 1995; Marques and Cobbold, 1995; Pennacchioni et al., 2000; Mancktelow et al., 2002; Ceriani et al., 2003; Schmid and Podladchikov, 2004, 2005; Mandal et al., 2005; Mulchrone, 2007; Johnson et al., 2009), large clast size compared to the width of the shear zone (Marques and Coelho, 2001), and interaction among clasts (Ildefonse et al., 1992a, b; Marques and Bose, 2004; Mandal et al., 2005). Third, extrapolating the kinematics of a small scale to that of a regional scale essentially assumes that deformation kinematics is uniform across scales many orders of magnitude different, ignoring the heterogeneous nature of rock deformation and deformation partitioning (e.g., Lister and Williams, 1983).

In addition to the strict assumptions mentioned above, to apply the vorticity analysis to natural shear zone also requires that all clasts be spheroidal or oriented in certain directions initially. However, these clasts are rare in nature. In this paper, using the algorithm of Jiang (2007) for modeling the rotation of rigid clasts in Newtonian viscous flows, we investigate fabrics defined by a population of arbitrarily shaped and initially randomly oriented clasts to critically examine those vorticity analysis methods using rigid clasts. We consider isochoric plane-straining flows and Sanderson-and-Marchini type transpressional (S&M) flows (Sanderson and Marchini, 1984) in this paper, because these two types of flow are mostly studied in the literature and the results from the study of them are sufficient to make our points. We show that even if the assumptions for vorticity analysis, as discussed above, are all accepted, and the bulk flow is simply monoclinic, the uncertainties associated with these methods are intrinsically too large for the results to be useful. The large uncertainties are due to the three dimensional (3D) nature of clast motion and cannot be eliminated. Reported vorticity numbers from these methods are normally in the range of 0.5–0.85 which have been used to argue that the hosting zones deviate significantly from simple shearing zones (e.g., Wallis et al., 1993; Xypolias and Koukouvelas, 2001; Law et al., 2004; Jessup et al., 2006; Sarkarinejad and Azizi, 2008; Frassi et al., 2009; Langille et al., 2010). Our numerical modeling shows that the reported range could all be from zones with close-to-simple-shearing flows.

2. Vorticity numbers

Ductile shear zones occur as highly deformed rocks bounded by far-less deformed or relatively undeformed wall rocks. The flow in such tabular zones is routinely and most conveniently described in a reference frame that is fixed to the zone-bounding country rocks. In this paper, we refer to a vertical, north–south trending shear zone and use a Cartesian coordinate system such that the X- and Y-axis are horizontal and pointing respectively to the north and east. The Z-axis is vertical and points down (Fig. 1a).

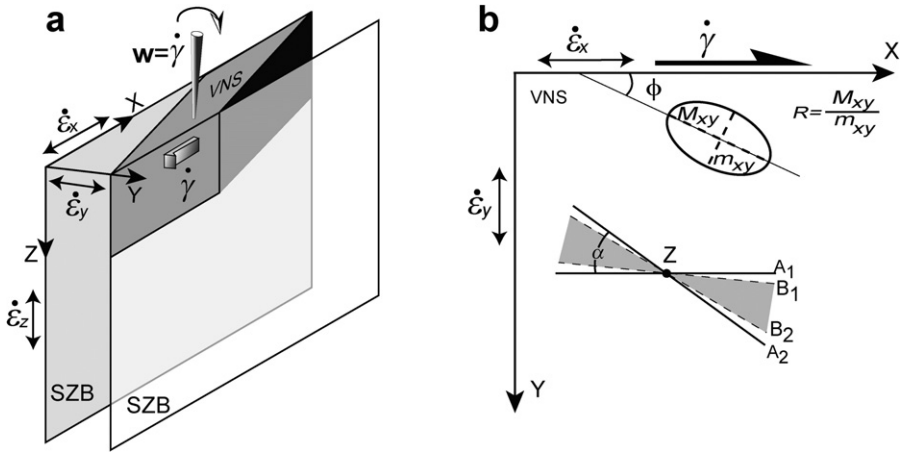

Fig. 1. (a) Reference frame, coordinate system and flow in a shear zone. The coordinate X-, Y-, and Z-axis point respectively to north, east, and down. The simple shearing component ($\dot{\gamma}$) is parallel to the X-axis. The vorticity vector **w** is parallel to Z-axis. The strain rates along X-, Y-, and Z-axis are $\dot{\varepsilon}_x$, $\dot{\varepsilon}_y$, and $\dot{\varepsilon}_z$ respectively. The vorticity-normal section (VNS) is on the XY-plane. SZB: shear zone boundary. For isochoric plane-straining flows, $\dot{\varepsilon}_x = -\dot{\varepsilon}_y$ and $\dot{\varepsilon}_z = 0$. For Sanderson-and-Marchini type transpressional (S&M) flows, $\dot{\varepsilon}_z = -\dot{\varepsilon}_y$ and $\dot{\varepsilon}_x = 0$. (b). Sectional flow on the VNS of a thinning zone ($\dot{\varepsilon}_y < 0$). Two flow apophyses are denoted by A_1, parallel to the shear direction, and A_2 inclined synthetically to the shear zone boundary at an acute angle α. Clasts viewed on the VNS are 2D ellipses whose major axis is M_{xy} and minor axis is m_{xy}. The aspect ratio of the ellipse is R ($= M_{xy}/m_{xy}$). In the special case where two symmetry axes of a 3D clasts are M_{xy} and m_{xy}, these two symmetry axes rotate on the VNS and R is constant. If the clast has $R > R_{crit}$, two orientations (stable orientation B_1:ϕ_1 and unstable orientation B_2:ϕ_2) exist for the clast. When the clast's M_{xy} axis is parallel to either, the clast has zero angular velocity. The clast's M_{xy} axis rotates away from B_2 toward B_1.

In our reference frame and coordinate system, the flows used in our modeling can be described by velocity gradient tensors of the forms:

$$\mathbf{L} = \begin{pmatrix} -\dot{\varepsilon}_y & -\dot{\gamma} & 0 \\ 0 & \dot{\varepsilon}_y & 0 \\ 0 & 0 & 0 \end{pmatrix} \text{(for isochoric plane-straining flows)} \tag{1a}$$

$$\mathbf{L} = \begin{pmatrix} 0 & -\dot{\gamma} & 0 \\ 0 & \dot{\varepsilon}_y & 0 \\ 0 & 0 & -\dot{\varepsilon}_y \end{pmatrix} \text{(for S\&M flows)} \tag{1b}$$

where $\dot{\gamma}(\dot{\gamma} > 0)$ is the shear strain rate for the simple shearing component and $\dot{\varepsilon}_y$ is the strain rate parallel to the *Y*-axis (Fig. 1a). The two types of flow can be in thinning zones ($\dot{\varepsilon}_y < 0$) or thickening zones ($\dot{\varepsilon}_y > 0$). We use thinning zones as examples to present our study in this section and the sections that follow, because they are common in nature. It should be noted that our conclusions drawn from modeling also hold for thickening zones. The eigenvectors of **L**, named flow apophyses (Ramberg, 1975a, b), are the orientations along which material lines have zero angular velocities. For the two types of flow (Eqs. (1a) and (1b)), there are three eigenvectors, two of which are on the XY-plane, and the third one is along the *Z*-axis (Fig. 1b).

The vorticity vector for the above two types of flow is

$$\mathbf{w} = \begin{pmatrix} 0 \\ 0 \\ \dot{\gamma} \end{pmatrix} \tag{2}$$

Because only steady flows (**L** is constant with time) are considered in this paper, the vorticity is entirely internal vorticity (Means et al., 1980; Lister and Williams, 1983; Tikoff and Fossen, 1995; Wallis, 1995; Jiang, 1999, 2010).

The plane normal to the vorticity vector **w** is called the vorticity-normal section (VNS, Jiang and Williams, 1998; Lin et al., 1998). It is a common practice to regard the section that shows the best fabric asymmetry in natural shear zones as the flow VNS. This practice can be justified if the flow is monoclinic (Passchier, 1998). Thus if a tectonite is from a more or less plane-straining shear zone, the section parallel to lineation and perpendicular to foliation is close to the flow VNS. For S&M flows, the VNS is either parallel to the lineation and perpendicular to the foliation or normal to the lineation.

There are two different kinematic vorticity numbers used in the literature. One was defined by Truesdell (1953, 1954), called the kinematic vorticity number or simply the vorticity number (Truesdell, 1991). For flows defined in Eqs. (1a) and (1b), the vorticity number is (see Jiang and Williams, 1998; Lin et al., 1998):

$$W_k = \frac{\dot{\gamma}}{\sqrt{4\dot{\varepsilon}_y^2 + \dot{\gamma}^2}} \tag{3}$$

Another number, often called the sectional (kinematic) vorticity number, was defined by Passchier (1987) and Robin and Cruden (1994). For our monoclinic flows, the sectional vorticity number W_k^s on the VNS is (see Robin and Cruden, 1994; Jiang and Williams, 1998; Lin et al., 1998):

$$W_k^s = \frac{\dot{\gamma}}{\sqrt{4\dot{\varepsilon}_y^2 + \dot{\gamma}^2}} \text{(for isochoric plane-straining flows)} \tag{4a}$$

$$W_k^s = \frac{\dot{\gamma}}{\sqrt{\dot{\varepsilon}_y^2 + \dot{\gamma}^2}} \text{(for S\&M flows)} \tag{4b}$$

The sectional vorticity number is related to the acute angle (α, Fig. 1b) of the two flow apophyses on the VNS by (Bobyarchick, 1986; Passchier, 1986):

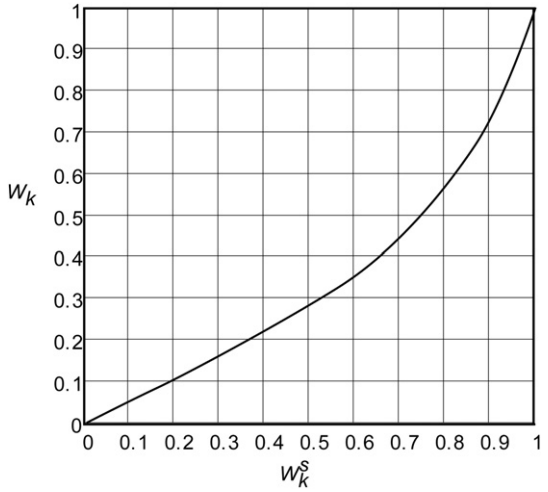

Fig. 2. Relationship between W_k and W_k^s in S&M flows.

$$W_k^s = \cos\alpha \tag{5}$$

In earlier studies of shear zones, only isochoric plane-straining deformations were considered (e.g., Ramsay and Graham, 1970; Ramberg, 1975b; Ramsay, 1980; Passchier, 1987; Simpson and De Paor, 1993) and it was sufficient to use the vorticity number of Truesdell (Eq. (3)) to completely characterize the kinematics of the flow. However, when 3D flows are investigated, a single Truesdell's vorticity number corresponds to an infinite number of possible flows (Tikoff and Fossen, 1995). It becomes necessary to distinguish flow kinematics viewed on the VNS from that of the 3D flow, and the sectional vorticity number W_k^s on the VNS was proposed to serve this purpose.

W_k^s differs from W_k except for isochoric plane-straining flows (Passchier, 1987, 1997; Robin and Cruden, 1994; Wallis, 1995; Eqs. (3) and (4a)). Fig. 2 shows their difference in S&M flows. It has been shown theoretically (e.g., Passchier, 1987; Appendix in Jiang, 2007) and is in fact justifiable by numerical modeling (see vorticity analysis methods and Fig. 4 in next section) that it is W_k^s rather than W_k that is relevant to rock fabrics observed on the VNS. Therefore it should be pointed out that what is obtained from vorticity analysis is W_k^s instead of W_k.

3. Vorticity analysis using rigid clasts

The motion of a rigid ellipsoidal clast in a viscous flow is a 3D problem described by a set of equations (Jeffery, 1922). The vorticity analysis methods using rigid clasts, however, are based on the application of Jeffery's theory to the following two very special cases in monoclinic flows: either all clasts must be spheroidal or, if they are triaxially shaped, must have one symmetry axis parallel to the vorticity vector of the flow. In the first case, analytical solutions to the Jeffery's equations exist (Ježek et al., 1996; Supplementary data in Jiang, 2007), and they show that given sufficiently large finite strain of the shear zone, the distinct axes of rigid clasts either rotate permanently following the so-called Jeffery's orbits or reach stable orientations (Jeffery, 1922; Passchier, 1987; Supplementary data in Jiang, 2007). Therefore, if stabilized clasts can be identified from rocks, their shapes (often measured by clast aspect ratio *R*) and orientations can be used to calculate the vorticity number. In the second case, the clast rotation is reduced to the two-dimensional (2D) problem of Ghosh and Ramberg (1976) which can be examined on the VNS (Passchier, 1987; Simpson and De Paor, 1993). Current vorticity analysis

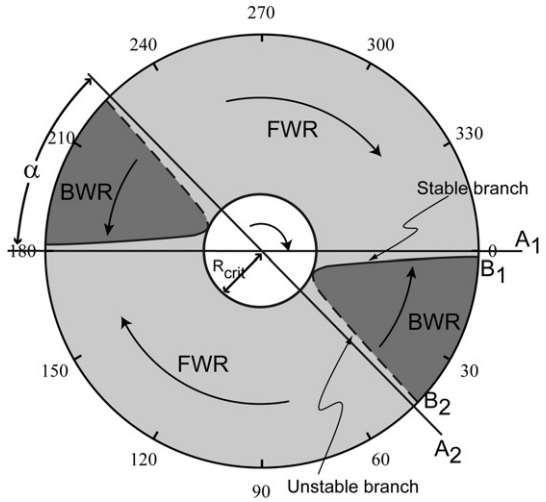

Fig. 3. 2D clast rotation behaviors in a R–ϕ plot in a polar coordinate. For any given W_k^s, a hyperbola (clast apophyses) can be constructed using Eqs. (7) and (8). The hyperbola approaches the flow apophyses (A_1 and A_2) asymptotically. Clasts plotted in the white area ($R < R_{crit}$) rotate permanently with vorticity; clasts plotted in the light grey area rotate forward until they reach their stable positions (on the solid branch of the hyperbola) while clasts plotted in the dark grey area rotate against vorticity (away from the dashed branch of the hyperbola) until they reach their stable positions (on the solid branch of the hyperbola). FWR: forward rotation. BWR: backward rotation.

methods using rigid clasts are mostly based on the 2D theory of Ghosh and Ramberg (1976) which we review briefly below in the context of vorticity analysis.

A clast viewed on a VNS is an ellipse whose major and minor axes are denoted by M_{xy} and m_{xy} ($M_{xy} \geq m_{xy}$; Fig. 1b). The shape of the ellipse is measured by the aspect ratio $R(= M_{xy}/m_{xy})$, and the orientation of the ellipse is measured by the angle ϕ between the M_{xy} axis and the shear plane (Fig. 1b). In the event that one of the three symmetry axes (a_1, a_2, and a_3, $a_1 \geq a_2 \geq a_3$) of a clast is parallel to the vorticity vector, the two remaining ones are on the VNS and are the M_{xy} and the m_{xy}. If the flow is simple shearing, the two symmetry axes M_{xy} and m_{xy} shall rotate permanently with vorticity, and if the flow is pure shearing, the two symmetry axes will finally stabilize with M_x and m_{xy} parallel to the two principal strain rate axes of the flow (Gay, 1968). In a general 2D monoclinic flow, a critical aspect ratio R_{crit} exists (Ghosh and Ramberg, 1976; Passchier, 1987):

$$R_{crit} = \sqrt{(1 + W_k^s)/(1 - W_k^s)} \quad (6)$$

whereby a clast with $R < R_{crit}$ rotates permanently with vorticity (forward rotation), and a clast with $R > R_{crit}$ will reach a stable orientation (Ghosh and Ramberg, 1976; Passchier, 1987). There are two orientations along which a clast with $R > R_{crit}$ has zero angular velocity:

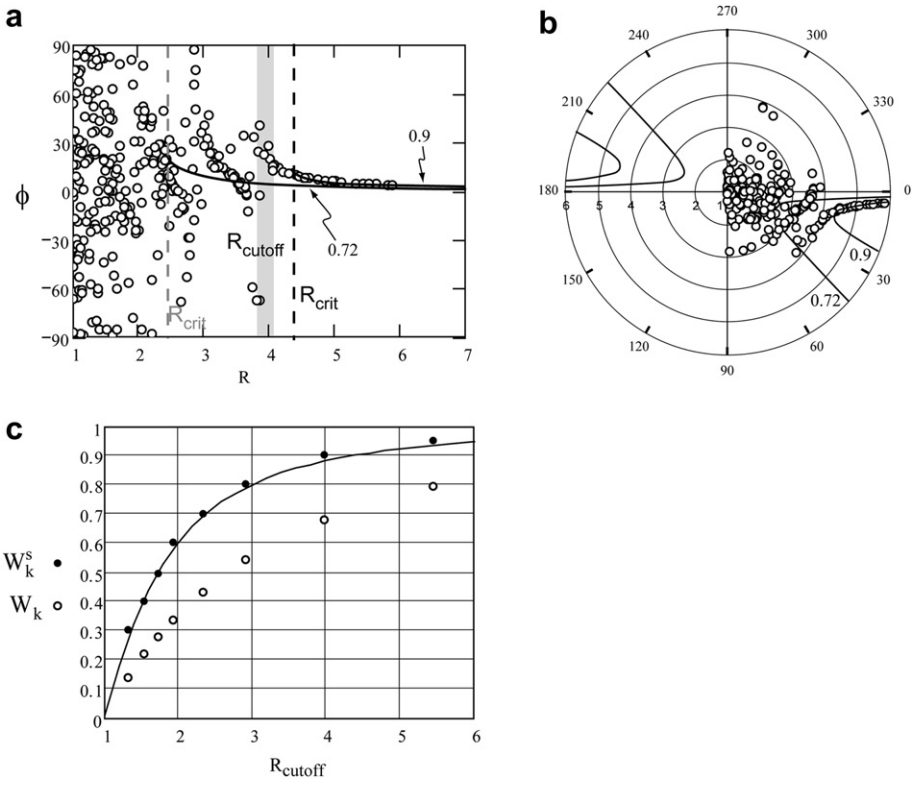

Fig. 4. Relationship between clast shape fabrics, W_k^s, and W_k, investigated by numerical experiments. All clasts have their a_1 axes parallel to the vorticity vector throughout deformation and their a_2 and a_3 axes are initially randomly oriented on the VNS. The clast shapes are shown in Fig. 5d. (a) and (b): R–ϕ plots of 300 clasts in an S&M flow with W_k^s of 0.9 ($W_k = 0.72$) at a high finite strain (ratio of the maximum over minimum principal stretch $s_1/s_3 = 7.4 \times 10^{10}$). Such an enormously high finite strain is adopted here to ensure that clasts with $R(=a_2/a_3) > R_{crit}$ reach their stable orientations. Shaded area in (a) indicates the possible range of R_{cutoff} following common vorticity analysis practice. The black dash line corresponds to a theoretical R_{crit} for a vorticity number of 0.9, and the grey one corresponds to a theoretical R_{crit} for a vorticity number of 0.72. Here the shaded area is close to the black dash line, suggesting that estimated vorticity number approximates actual W_k^s with the ARC method. The curves in (a) and hyperbolas in (b) are constructed using Eqs. (7) and (8), and the corresponding vorticity numbers are indicated beside. Clasts with large R's are plotted along the curve in (a) and the hyperbola in (b) both for the vorticity number of 0.9, suggesting that it is W_k^s estimated in the SC method. (c) Results from a series of numerical experiments for S&M flows. Again, extremely high strains (impossible in any natural shear zone) are adopted in our experiments here. Solid circles represent R_{cutoff} for corresponding W_k^s. The W_k corresponding with W_k^s are represented by open circles. The curve is constructed using Eq. (6) with the assumption that $R_{cutoff} = R_{crit}$. All solid circles instead of open circles lie on the curve, suggesting that it is W_k^s instead of W_k that is related to clast shape fabrics observed on the VNS.

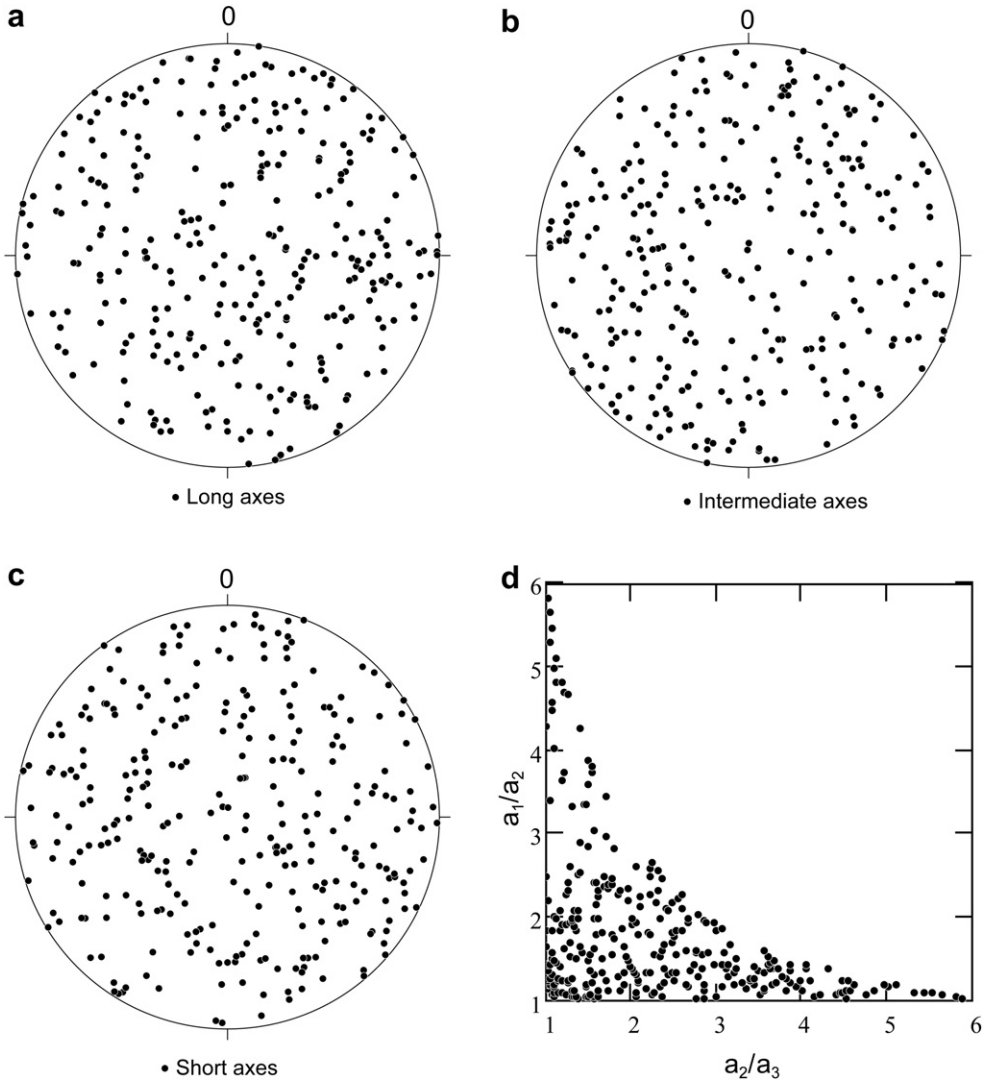

Fig. 5. (a–c) Lower-hemisphere equal-area projections of the initial orientations of the symmetry axes of 300 clasts generated for numerical modeling. (d) Flinn plot for the shapes of the clasts. See text for more details.

$$\phi_1 = \frac{1}{2}\left\{\arccos\left(W_k^s\right) - \arccos\left[\frac{\left(R^2+1\right)W_k^s}{R^2-1}\right]\right\}, \tag{7}$$

$$\phi_2 = \frac{1}{2}\left\{\arccos\left[\frac{\left(R^2+1\right)W_k^s}{R^2-1}\right] + \arccos\left(W_k^s\right)\right\} \tag{8}$$

The ϕ_1 orientation is shown in Fig. 1b as B_1 and the ϕ_2 orientation is shown as B_2. The ϕ_1 orientation is the stable orientation toward which the M_{xy} axis rotates. The ϕ_2 orientation is an unstable orientation from which the M_{xy} axis rotates away (Ghosh and Ramberg, 1976; Passchier, 198., 1995). The rotation behaviors are best represented in a polar coordinate system of R against ϕ (Simpson and De Paor, 1993; Fig. 3). For a given flow (W_k^s known), ϕ_1 and ϕ_2 are functions of R and Eqs. (7) and (8) define a hyperbola in a polar coordinate plot of R against ϕ. Clasts from a shear zone plotted on the corresponding hyperbola have zero angular velocities. Similar to flow apophyses for material lines, these hyperbolas can be called "clast apophyses". The two asymptotic lines of the "clast apophyses" correspond to the two apophyses for material lines. As shown in Fig. 3, clasts plotted within the $R = R_{crit}$ circle rotate permanently, while those plotted outside of the circle ($R > R_{crit}$) can reach stable orientations. Clasts plotted within the concave side of the hyperbola rotate backward (against vorticity), while those plotted outside rotate forward (with vorticity).

In vorticity analysis using rigid clasts, R–ϕ data are first plotted in a Cartesian coordinate system or a polar coordinate system, and three methods have been used (Passchier, 1987; Simpson and De Paor, 1993; Wallis et al., 1993). In the first method, here called the 'aspect ratio cutoff' (ARC) method, a dividing line (for a Cartesian R–ϕ plots) or circle (for a polar R–ϕ plots) is determined from such a plot that separates the domain with a wide range of ϕ values (interpreted as representing permanently-rotating clasts) from the domain showing a narrow range of ϕ values (taken to represent stable clasts). We call the R value corresponding to this dividing line (or circle) R_{cutoff}. R_{cutoff} has been regarded as R_{crit} in the calculation of vorticity using Eq. (6). We shall demonstrate later that this is not appropriate. The second method, here called the 'stabilized clast' (SC) method, is to identify clasts that are believed to have reached their stable orientations and then Eq. (7) is used to calculate the vorticity number. The third method here called the 'backward rotating clast' (BRC) method is to identify backward rotating clasts from forward rotating ones and plot both groups with different

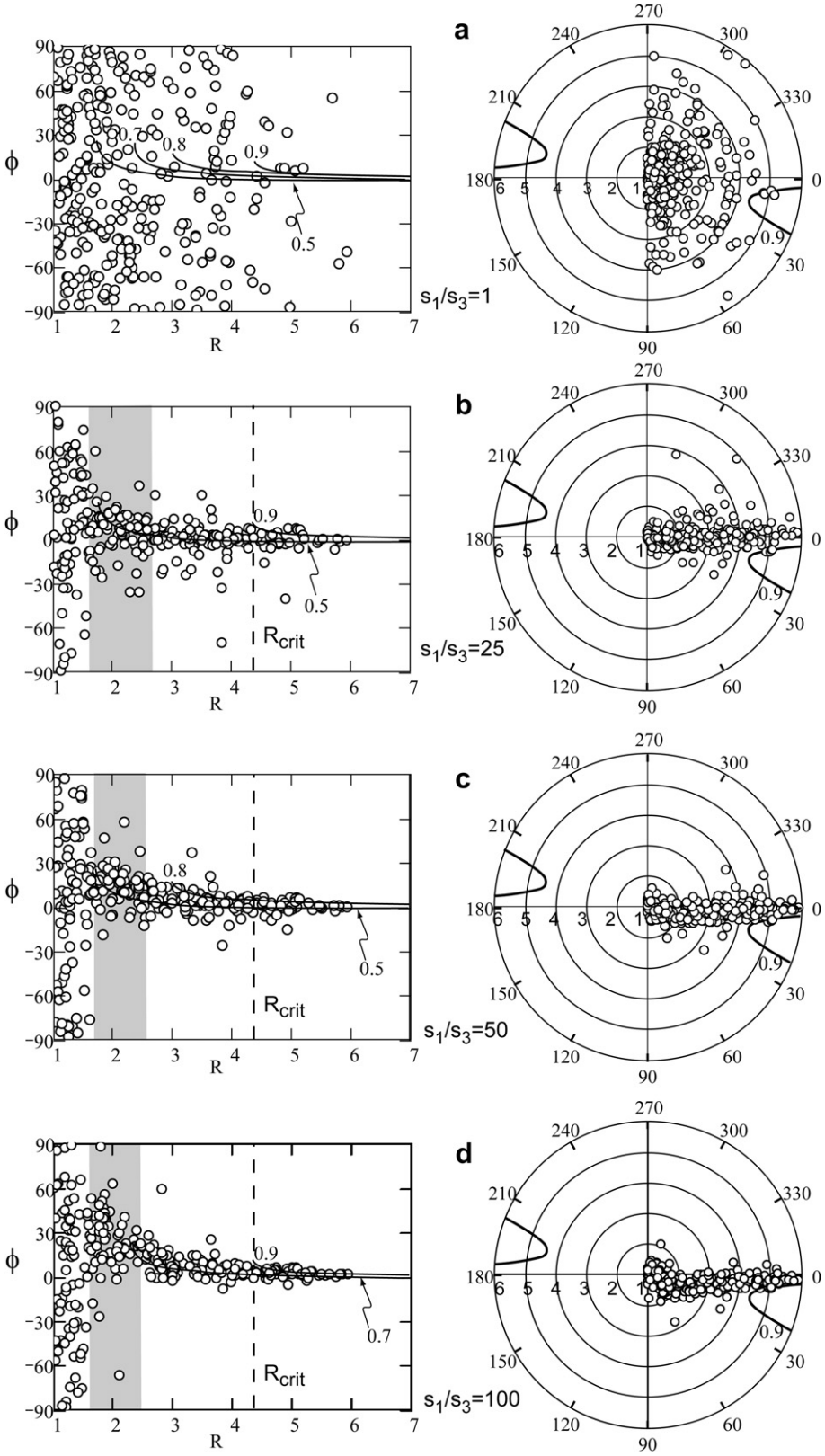

Fig. 6. $R-\phi$ plots for a plane-straining flow with W_k^s of 0.9, at different bulk finite strains. The curves in the Cartesian plots are constructed using Eq. (7), and the corresponding W_k^s values are indicated beside. The hyperbolas in the polar plots are constructed using Eqs. (7) and (8) for the W_k^s of 0.9. All clasts are forward rotating. Shaded areas indicate the possible range of R_{cutoff} following common vorticity analysis practice.

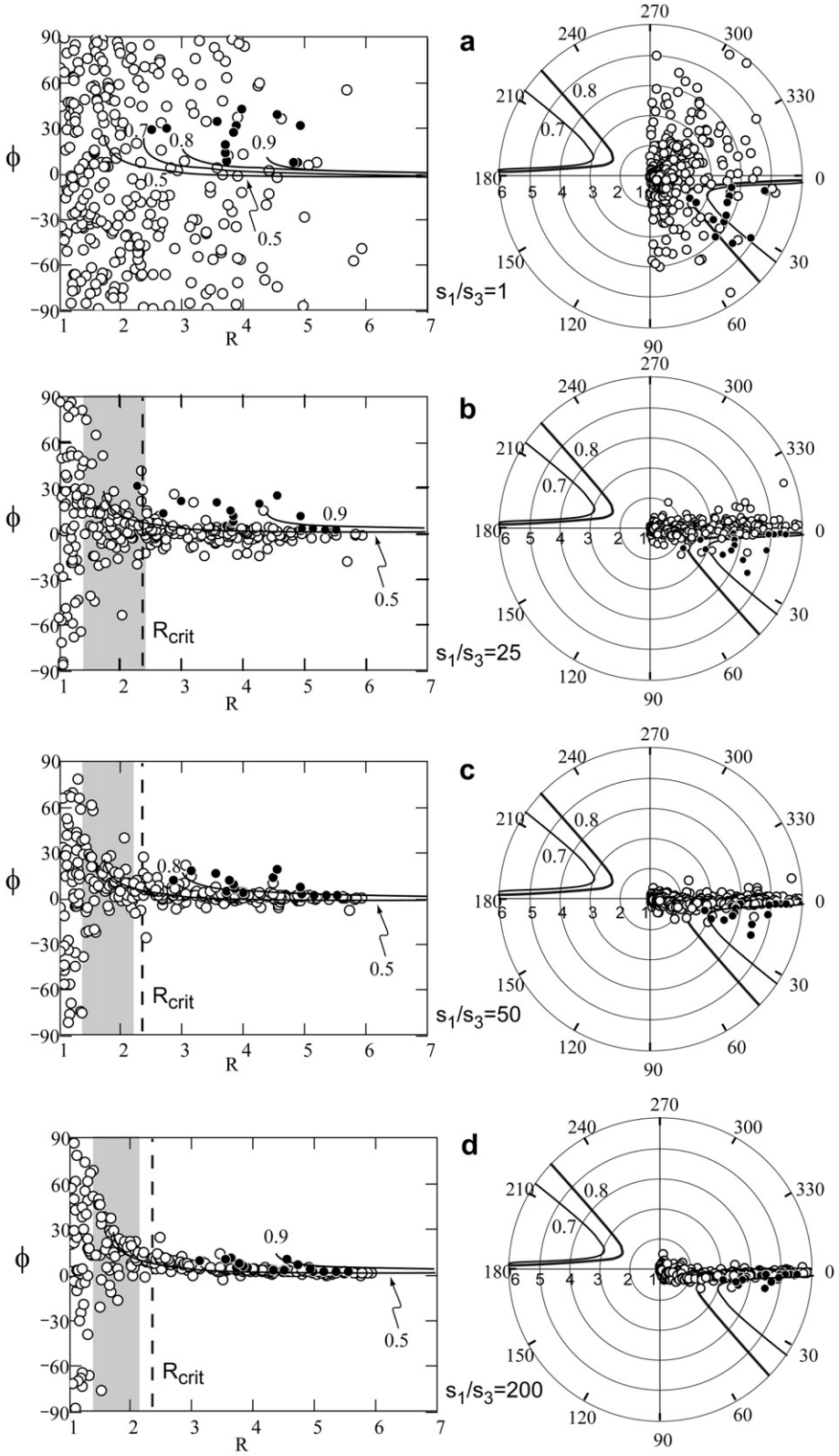

Fig. 7. $R-\phi$ plots for a plane-straining flow with W_k^s of 0.7 at different bulk finite strains. The curves in Cartesian plots are constructed using Eq. (7). The two hyperbolas in the polar plots are constructed using Eqs. (7) and (8). One is for a W_k^s of 0.7 and the other is for a W_k^s of 0.8. Forward rotating clasts are plotted as open circles, while backward rotating clasts are plotted as black solid circles. Shaded areas indicate the possible range of R_{cutoff} following common vorticity analysis practice.

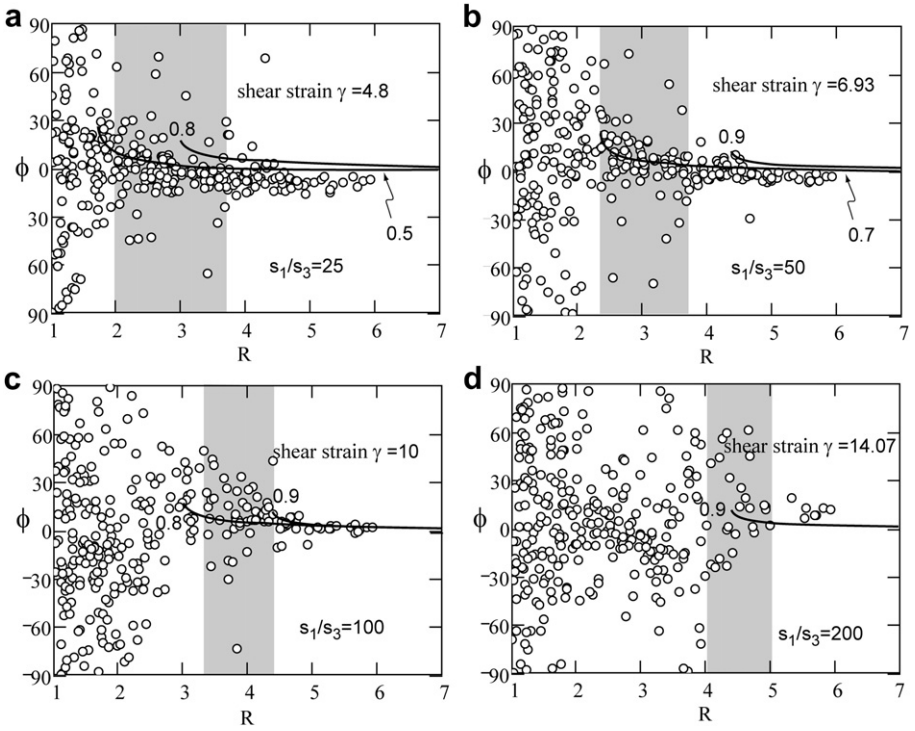

Fig. 8. $R-\phi$ Cartesian plots for a simple shearing flow ($W_k^s = 1$) at different bulk finite strains. All clasts are forward rotating. The R_{crit} for this flow is infinite. However, the R_{cutoff} is finite at different strains: 2.0–3.7, 2.36–3.7, 3.3–4.36, and 4–5, which would yield estimated vorticity numbers 0.6–0.86, 0.7–0.86, 0.83–0.9, and 0.88–0.92 respectively using the ARC method. With the SC method, the estimated vorticity numbers are 0.5–0.8, 0.7–0.9, 0.8–0.9, and >0.9. Note that the clast shape preferred orientation is not stable in the simple shearing (intensity decreases from (a) to (d)), and this is also observed in Ježek et al. (1994) and Ildefonse et al. (1997).

symbols in a polar coordinate $R-\phi$ diagram. The curve separating the two groups is then fitted to theoretical hyperbola in order to estimate the vorticity number.

With the $R-\phi$ polar coordinate plot being used, the three methods above, especially the BRC method, have been referred to as porphyroclast hyperbolic distribution (PHD) method (Simpson and De Paor, 1993). The ARC or SC methods used with a Cartesian coordinate plot have been referred to as the rigid grain net (RGN) method (Jessup et al., 2007), or the porphyroclast aspect ratio method (Passchier, 1987; Wallis et al., 1993).

For the ARC method, the uncertainty in the estimated vorticity number depends on how well R_{cutoff} can represent R_{crit} (Fig. 4a). For the SC method, the uncertainty lies on whether stabilized clasts are correctly identified. For the BRC method, the uncertainty depends on how well backward rotating clasts are correctly distinguished from forward rotating clasts, and how accurate the boundary line can be defined and fitted into a unique hyperbola.

All methods are based on the 2D theory of Ghosh and Ramberg (1976) which hardly applies directly to any rock deformation involving rigid clasts, because the motion of natural rigid clasts is intrinsically a 3D problem. Uncertainties associated with 3D nature of rigid clast motion are previously unknown. We now analyze the level of uncertainty by numerical modeling.

4. Numerical modeling

Although rigid clast fabrics used for vorticity analysis have to be obtained on 2D sections like the VNS, rigid clast motion in 3D flows must be dealt with three dimensionally. Since no analytical solutions to Jeffery's equations for general cases exist (Freeman, 1985; Ježek et al., 1994), we now apply numerical modeling to address the 3D motion of rigid clasts in general monoclinic flows described by the velocity gradient tensor of Eqs. (1a) and (1b). We investigate the shape fabric of the rigid clasts that will develop and evolve on the VNS as deformation advances and examine the consequences of applying this shape fabric for vorticity analysis using each of the three methods reviewed above. Our numerical modeling is based on Jiang (2007). The numerical modeling method can investigate clast shape fabric evolution in 3D or as observed on any specified section such as the VNS so that direct comparison between modeling results and geological observations can be made readily.

4.1. Generation of the initial population of rigid clasts

We generate a population of 300 clasts with uniform randomly distributed initial orientations (Fig. 5a–c) like previous studies (e.g., Freeman, 1985; Ježek et al., 1996) following the procedure of Jiang (2007). For their shapes (symmetry axes: $a_1 \geq a_2 \geq a_3$), we first generate a random number between 1 and 6 for the ratio (r) of a_1/a_3 for each clast and then generate a random number between 1 and r for the ratio a_2/a_3 of that clast. The shapes for this population of clasts generated are plotted in a Flinn diagram in Fig. 5d.

4.2. Numerical modeling of a population of rigid clasts and its implication

We investigated clast fabrics developed in our two types of flows. For plane-straining flows we modeled 3 cases, with W_k^s (=Wk for plane-straining situations) being respectively 0.9, 0.7 and 1. The $R-\phi$ patterns on the VNS ($R-\phi$ plots) for each case at different finite strain states are presented in Figs. 6–8 respectively. For S&M flows, we modeled two cases with W_k^s of 0.9 and 0.7. The

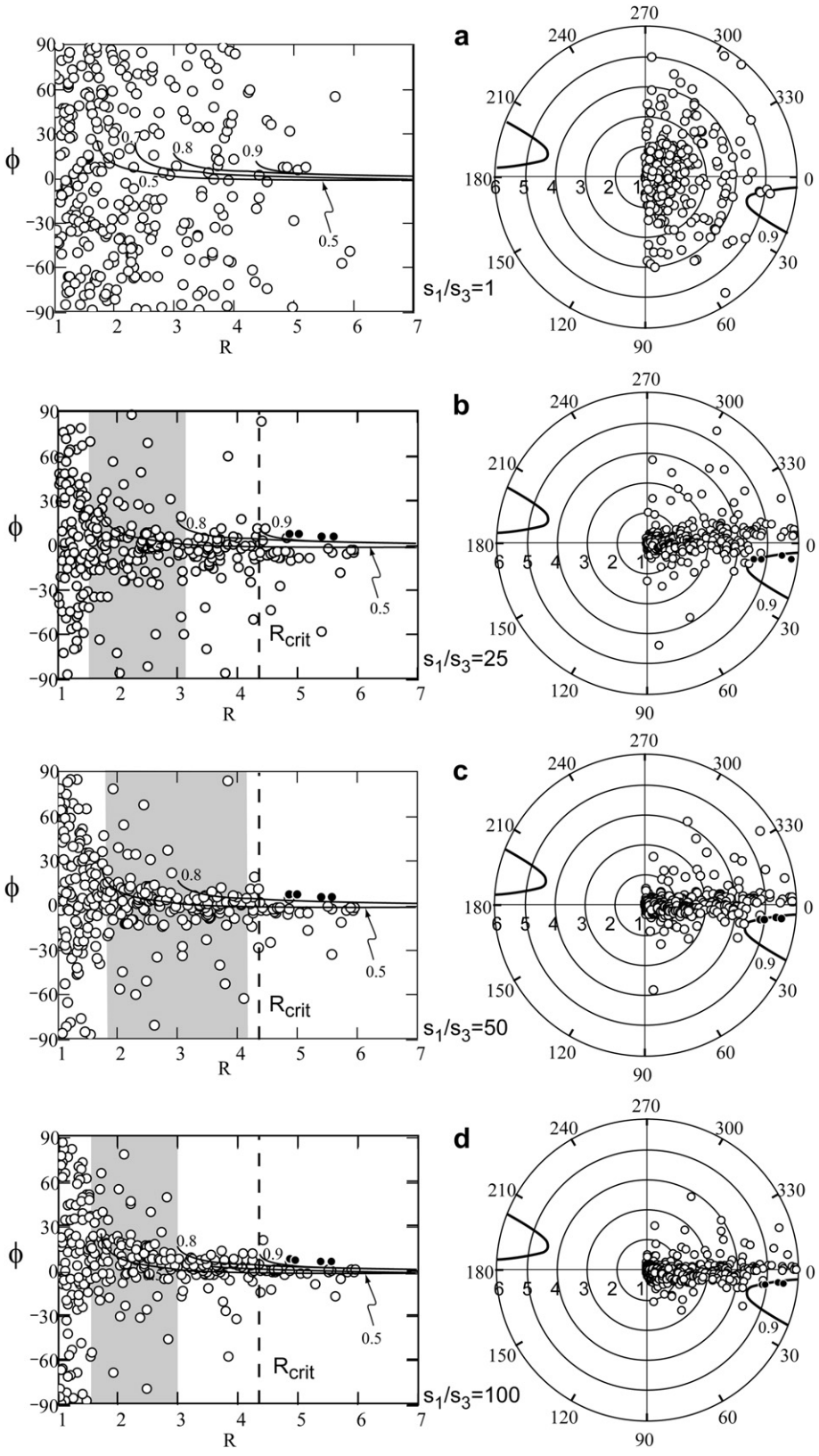

Fig. 9. $R-\phi$ plots for an S&M flow with W_k^s of 0.9 at different bulk finite strains. Symbols are the same as in Fig. 7.

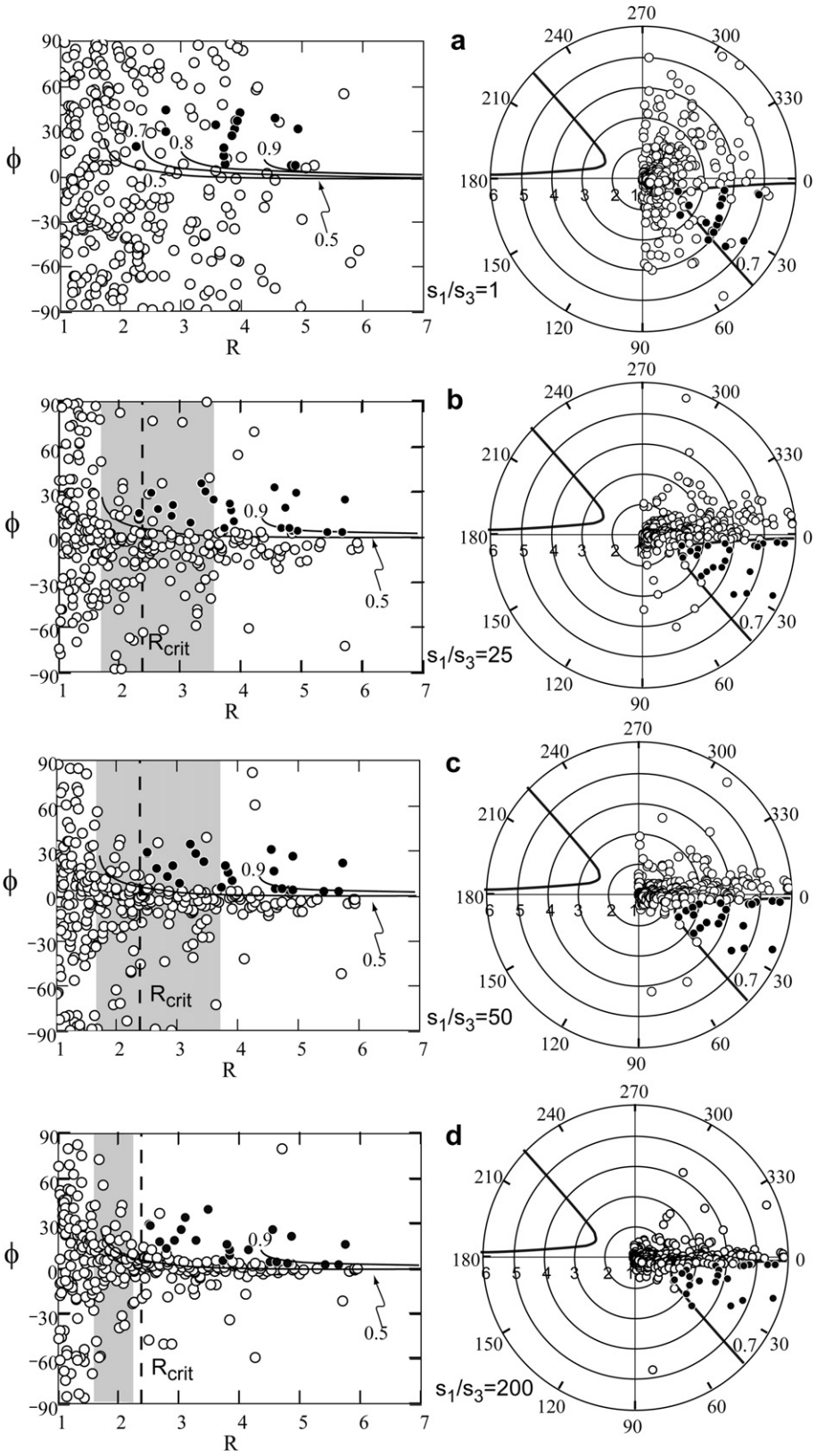

Fig. 10. $R-\phi$ plots for an S&M flow with W_k^s of 0.7 at different bulk finite strains. Symbols are the same as in Fig. 7.

resulting $R-\phi$ patterns on the VNS at different finite strain states for each case are presented in Figs. 9 and 10 respectively. We now test each of the three vorticity analysis methods.

4.2.1. The aspect ratio cutoff (ARC) method

Fig. 6 shows the $R-\phi$ plots for a plane-straining flow with W_k^s of 0.9 which gives a theoretical R_{crit} of 4.36. The R_{cutoff} that one would obtain following the common practice (e.g., Wallis et al., 1993; Law et al., 2004) from these $R-\phi$ plots would be like 1.6–2.7, 1.7–2.6, and 1.6–2.5 at bulk finite strains (ratio of the maximum principal stretch over the minimum principal stretch s_1/s_3) 25, 50, and 100 respectively. They would yield estimated vorticity numbers 0.44–0.76, 0.49–0.74, and 0.44–0.72 respectively. Fig. 9 presents the $R-\phi$ plots for an S&M flow with W_k^s of 0.9 corresponding to a theoretical R_{crit} of 4.36. The R_{cutoff} from these $R-\phi$ plots are 1.5–3.2, 1.8–4.2, and 1.6–3.0 at bulk finite strains (s_1/s_3) 25, 50, and 100 respectively, which would yield estimated vorticity numbers of 0.38–0.82, 0.53–0.89, and 0.44–0.80 as opposed to the actual W_k^s = 0.9 of the flow. Fig. 8 presents $R-\phi$ plots for a simple shearing flow, and the estimated vorticity numbers are in the range of 0.6–0.92. Fig. 7 presents $R-\phi$ plots for a plane-straining flow and Fig. 10 for an S&M flow both with a given W_k^s of 0.7. The estimated vorticity numbers from clast shapes on the VNS are in the range of 0.32–0.87.

4.2.2. The stabilized clast (SC) method

This method highly depends on how well stabilized clasts are correctly identified from natural mylonites. In the Cartesian $R-\phi$ plots, it is a common practice to use clasts with large R's to best fit a hyperbola defined by Eq. (7) to estimate the W_k^s. Fig. 6b–d shows that in a plane-straining flow (W_k^s = 0.9) the method would yield estimated vorticity numbers of 0.5–0.9, 0.5–0.8, and 0.7–0.9 respectively at different finite strains. Fig. 9b–d shows that in an S&M flow (W_k^s = 0.9) the estimated vorticity numbers are 0.5–0.9, 0.5–0.8, and 0.5–0.9 respectively at different finite strains. In these examples the W_k^s is underestimated, and the uncertainty can be as large as 0.4 as shown in Figs. 6b and 9b. Fig. 8 presents $R-\phi$ plots for a simple shearing flow, and the estimated vorticity numbers are in the range of 0.5–1.0. High uncertainty in estimated vorticity number is also shown in numerical modeling of the plane-straining flow (W_k^s = 0.7, Fig. 7b–d) and the S&M flow (W_k^s = 0.7, Fig. 10b–d), from both of which the estimated vorticity numbers are in the range of 0.5–0.9.

4.2.3. The backward rotating clast (BRC) method

This method requires that backward rotating clasts can be identified. Clast rotation in 3D space is much more complicated than the 2D theory of Ghosh and Ramberg. The angular velocity vector **ω**, describing the instantaneous rotation for an individual clast, can have any angle between 0° and 180° with respect to the vorticity vector **w**. A clast as a whole is momentarily rotating forward if the angle between **ω** and **w** is acute and backward if it is obtuse. Figs. 7a and 10a show that, unlike 2D situations where forward and backward rotating clasts are separated by the hyperbolic clast apophyses, in 3D cases on the VNS forward and backward rotating clasts can be mixed together and that no distinct boundary exists between the two groups. If we ignore the forward rotating clasts and draw a hyperbola to closely enclose all the backward rotating clasts, this hyperbola would correspond to a vorticity number less than 0.7 (actual W_k^s of the flows). Fig. 7c and d indicate that the estimated vorticity numbers is 0.8, which is higher than the actual W_k^s (=0.7). Figs. 6a–d and 9a show no backward rotating clasts, which would imply an estimated vorticity number of 1, while the actual W_k^s is 0.9.

Our numerical modeling above suggests that large uncertainties exist in estimating vorticity numbers using rigid clasts. Considering this level of uncertainty, reported vorticity numbers in the literature in the range of 0.5–0.85 using the ARC and SC methods may come from flow fields that are all close to simple shearing.

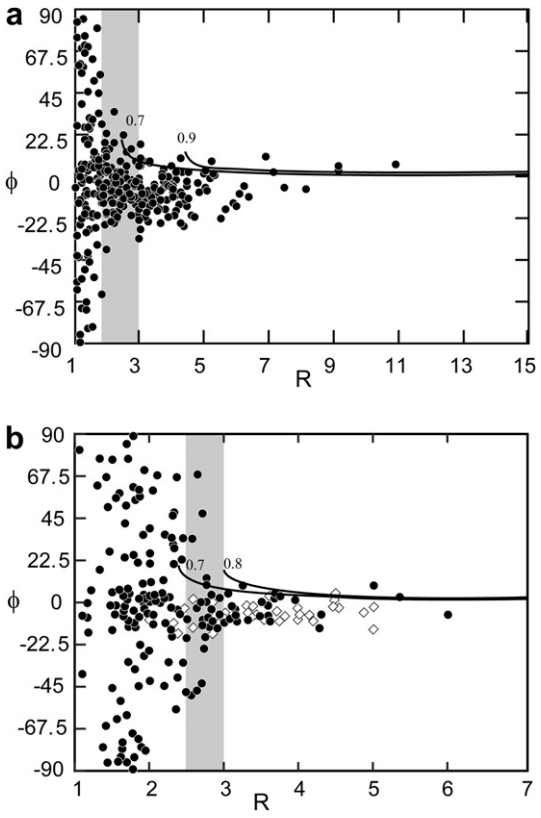

Fig. 11. $R-\phi$ Cartesian coordinate plots of natural clast data. (a) Clasts of feldspar from the Okanagan Valley shear zone, BC, Canada. (b) Data taken from the first plot of fig. 10 in Law et al. (2004). Black circles represent feldspars, and white squares represent amphiboles.

$R-\phi$ patterns from many natural shear zones have been presented in the literature (e.g., fig. 13 in Wallis et al., 1993; fig. 6 in Xypolias and Koukouvelas, 2001; fig. 10 in Law et al., 2004; fig. 5 and figs. A1–A5 in Jessup et al., 2006; fig. 10 in Sullivan, 2008; fig. 9 in Frassi et al., 2009; fig. 7 in Johnson et al., 2009). They all look similar to our modeling-produced patterns. Here, we take two natural examples to illustrate that estimated vorticity numbers in the range of 0.5–0.85 may all have come from flow fields that are close to simple shearing. One is from mylonites in the Okanagan Valley shear zone in British Columbia, Canada. Kinematic analysis and field geology of the shear zone suggest that the deformation path is close to simple shearing (Liu, 2009). Fig. 11a is the $R-\phi$ plot of the clasts collected from the Okanagan Valley shear zone, and it suggests a R_{cutoff} of 1.8–3, which would yield an estimated vorticity number of 0.53–0.8 using the ARC method. Using the SC method, the estimated vorticity number is in the range of 0.7–0.9. The other example is shown in Fig. 11b, taken from Law et al. (2004, the first plot of their fig. 10). The R_{cutoff} is 2.5–3.0, which would yield an estimated vorticity number of 0.72–0.8 using the ARC method. With the SC method, the estimated vorticity number would be between 0.7 and 0.8. The $R-\phi$ plots from the above two examples as well as those from many other natural shear zones are similar to our modeling results (Fig. 6b–d and Fig. 9b–d). Therefore, like our numerical modeling results, the vorticity numbers estimated from these natural shear zones could also have been produced by close-to-simple-shearing flows.

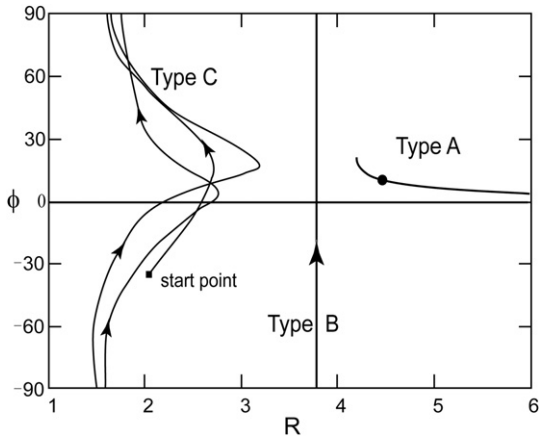

Fig. 12. $R-\phi$ Cartesian coordinate plot of rotation paths for three types of clasts. At sufficiently high strains type A clasts stabilize, and they are plotted on the curve in the $R-\phi$ plot. At sufficiently high strains, a type B clast, having one symmetry axis parallel to the vorticity vector, only changes its ϕ. A type C clast always changes its R and ϕ with deformation, and shows complicated trajectory of $R-\phi$ path. The R of this clast is always less than its $a_1/a_3(=3.5)$.

5. Why are the uncertainties so large?

We have shown above that even in the ideal modeling situations (given monoclinic, homogeneous and steady flow, all clasts obeying Jeffery's theory), the estimated vorticity numbers generally have uncertainties so large that all currently reported numbers (0.5–0.85) could have been explained by simple shearing. It is unnecessary, from the estimated "vorticity numbers" alone, to invoke shear zone boundary conditions significantly different from simple shearing. Why are the uncertainties so large? We will show in this section that these uncertainties are due to the 3D nature of rigid clast rotation. They are intrinsic and cannot be removed by any "better" measurements or presentations of the observable dataset.

In order to understand the nature and origin of the uncertainties, it is necessary to investigate rotation behavior of individual triaxially-shaped clasts in monoclinic flows. The 3D rotation is complex. To facilitate discussion, we divide clasts in monoclinic flows into three types according to their rotation behaviors (Fig. 12).

5.1. Clast rotation behaviors

A clast is type A if it can reach a stable orientation where all of its three symmetry axes are fixed. When it reaches the stable orientation, both its shape (R) and orientation (ϕ) are fixed on the VNS. A clast is type B if it rotates permanently but will eventually have one symmetry axis parallel to the vorticity vector. Once one symmetry axis of a type B clast reaches parallelism with the vorticity vector, its R on the VNS is fixed, but its ϕ still varies with deformation. A clast is type C if it rotates permanently and none of its symmetry axes is parallel to the vorticity vector. For a type C clast, both its R and ϕ on the VNS vary with deformation. In a given general monoclinic flow, what type of behavior an ellipsoidal clast follows depends on the flow field and the clast shape. For a type A or type B clast, the symmetry axis that eventually aligns with the vorticity vector is its intermediate axis if the flow field is a plane-straining one and its long axis if the flow field is an S&M flow. Fig. 13 shows the relation between clast shape and clast rotation type in plane-straining general flows and S&M flows. In a plane-straining flow field, a clast with $a_1/a_3 > R_{crit}$ is a type A clast because it can stabilize with its intermediate principal axis parallel to the vorticity vector. A clast with $a_1/a_3 < R_{crit}$ is a type C clast. In an S&M flow field, it is always the long axis of a clast that will eventually reach parallelism with the vorticity vector. The clast is type A if its $a_2/a_3 > R_{crit}$, and type B if its $a_2/a_3 < R_{crit}$.

Although in monoclinic flows a clast of type A or type B eventually has one symmetry axis parallel to the vorticity vector in principle, it is impossible for most of these clasts in a natural shear zone to reach the orientations if they are initially randomly oriented (Figs. 14 and 16). To align the symmetry axes of most of these clasts with the vorticity vector requires enormously high strains. For the sectional kinematic vorticity number in the range of 0.7-0.9, for example, the required finite strains would amount to reducing a 10-km-wide zone to one less than 10 cm wide! These strains are ridiculously too high for any natural shear zones.

5.2. Origin of uncertainties for each method

The 3D nature of clast rotation at geologically realistic strain leads to large uncertainties in the vorticity analysis methods. In plane-straining or S&M flows, ϕ values of clasts, especially elongated ones (mostly type A), tend to decrease to within 10° of the shear plane quite rapidly as deformation advances. But afterwards the ϕ values change very slowly with further deformation (Figs. 15 and 16b–d, f–h). Because of this, the R_{cutoff} can significantly differ from R_{crit}. In a flow approaching simple shearing, R_{crit} approaches infinity while R_{cutoff} is always a small finite number. Therefore the estimated vorticity number never quite reaches 1. The difference

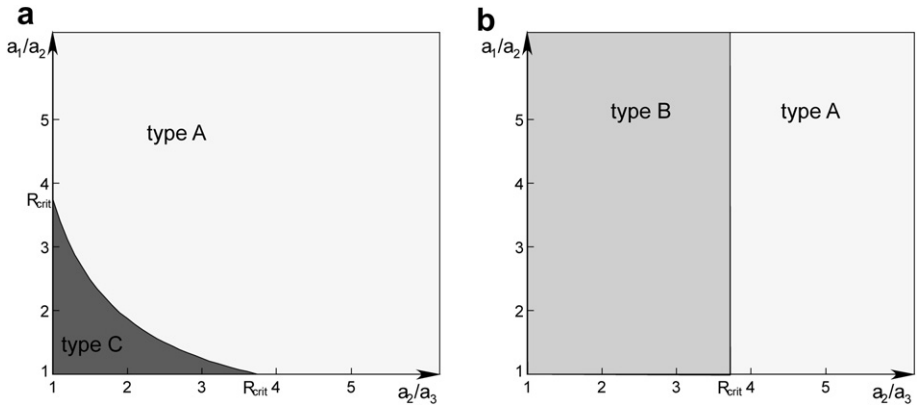

Fig. 13. Flinn diagrams showing the relation of clast rotation type to clast shape in two types of flows. (a) In a general plane-straining flow, clasts are either type A or type C. (b) In an S&M flow, clasts are either type A or type B.

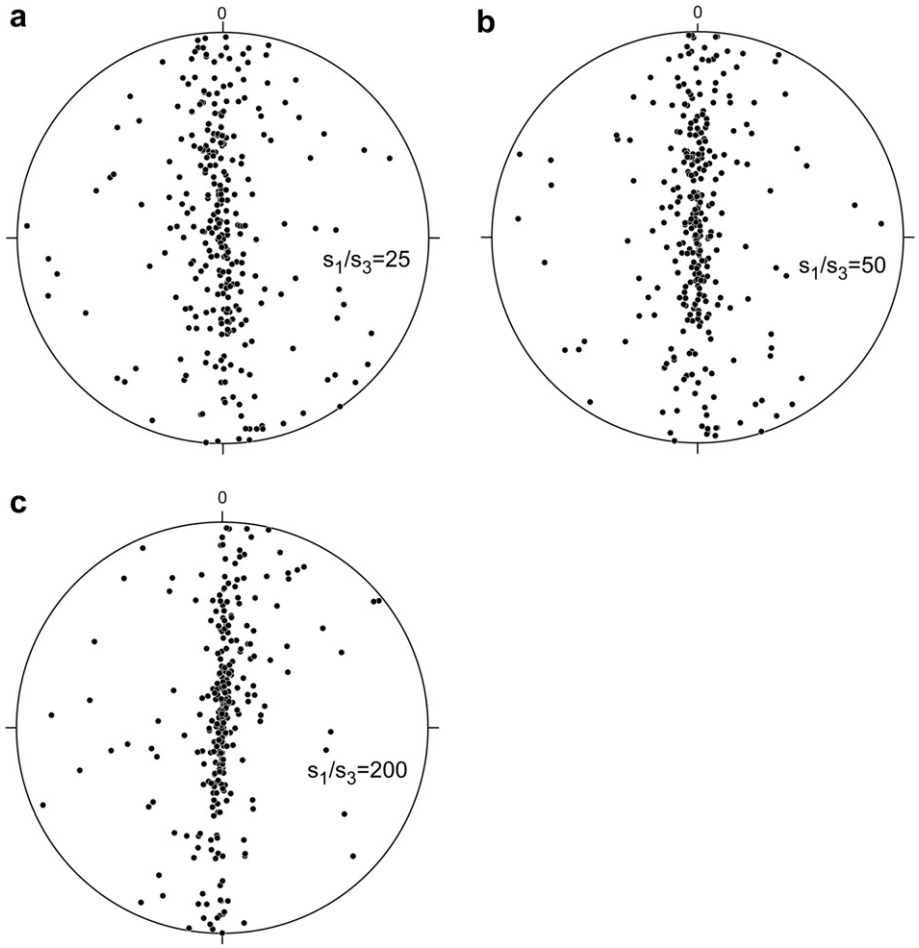

Fig. 14. Lower-hemisphere equal-area projections of the a_1 axes of 300 clasts at different bulk finite strains in the S&M flow with W_k^s of 0.9. All clasts are initially uniformly oriented (Fig. 5a-c), and their shapes are shown in Fig. 5d. Very few clasts can reach the orientations where their a_1 axes are parallel to the vorticity vector at geologically realistic strains. In (c) the shear zone width is already thinned to 14.3% of its original width; however, only 18.7% clasts align their a_1 axes to be within 10° to the vorticity vector.

between R_{crit} and R_{cutoff} can be very large, which leads to large uncertainties in the aspect ratio cutoff (ARC) method. For geologically realistic strain, very few clasts of type A can reach their stable orientations (Fig. 16). The linear curve defined by clasts with large R's may significantly differ from that defined by stabilized clasts on the R–ϕ plot, and it leads to a large uncertainty in the stabilized clast (SC) method.

In any S&M flow, it takes relatively small strain for the trends of a_1 axes of most clasts, especially elongated clasts, to approach the strike of the shear zone boundary and for a_3 axes to approach the

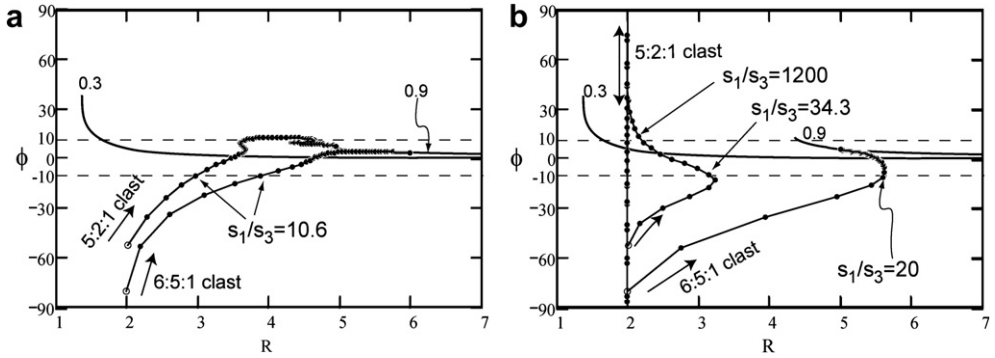

Fig. 15. R–ϕ rotation paths for two clasts both having the same initial orientation (long axis: 12°, 137°, intermediate axis: 13°, 230°, and short axis: 72°, 105°) in the plane-straining flow (a) and the S&M flow (b) both with W_k^s of 0.9. The initial states of the two clasts are plotted as open circles. Note that for either clast, ϕ decreases quickly to be within 10° of the shear plane and then changes very slowly. In a S&M flow, only after a_1 axis reaches parallelism with the vorticity vector, a type B clast starts to show a wide range of ϕ values (the 5:2:1 clast in (b)). The two curves in both (a) and (b) are constructed using Eq. (7) for a vorticity number of 0.3 and 0.9 respectively. At geologically realistic strains, if these two clasts are treated as stabilized clasts, the estimated vorticity number will be 0.3–0.9, using the SC method.

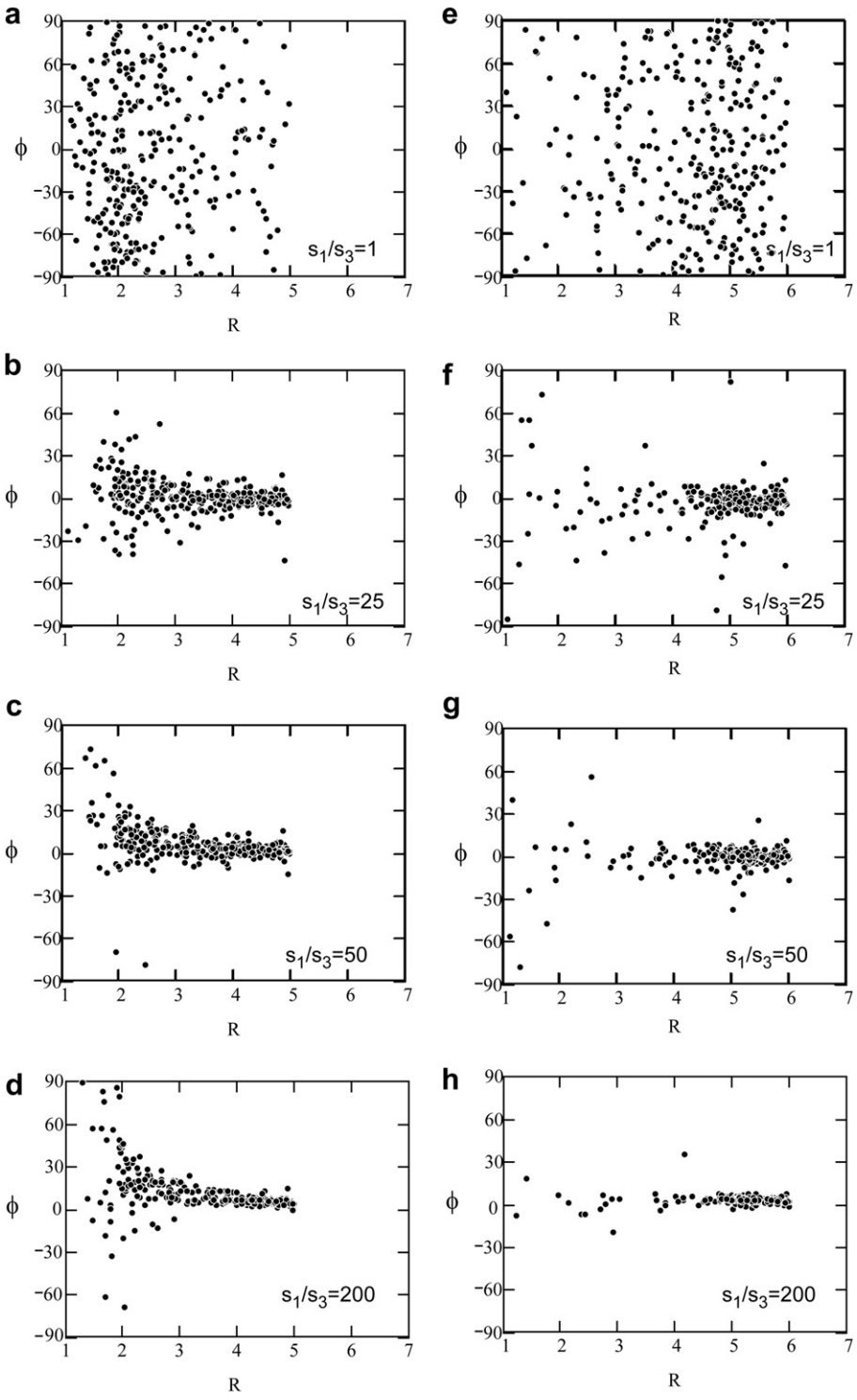

Fig. 16. R–ϕ Cartesian coordinate plots of 300 clasts in the plane-straining flow with W_k^s of 0.9. All clasts are initially uniformly oriented (Fig. 5a-c), but their shapes in (a–d) are a_1:a_2:a_3 = 5:2:1, and in (e–h) are a_1:a_2:a_3 = 6:5:1. Note that these clasts start to show low ϕ values at relatively low finite strain (b and f). Both of the two types of clasts are type A, and in principle their intermediate axes will eventually align with the vorticity vector showing $R = 5$ for 5:2:1 clasts and $R = 6$ for 6:5:1 clasts in plots. However, very few clasts align their intermediate axes with the vorticity vector at bulk finite strain of $s_1/s_3 = 200$ when the shear zone width is thinned to 15.9% of its original width (d and h).

shear zone normal (Figs. 14 and 17). After that the plunges of a_1 axes increase gradually but the trends hardly change (Fig. 14). Therefore, on the VNS, clasts with large R's tend to show ϕ's around zero, but they are far from stabilized. With SC method, the uncertainty in estimated vorticity number by treating these clasts as stabilized clasts can be as large as 0.6 (Fig. 15). When the a_1 axes of type B clasts of $a_2/a_3 = R_1$ (R_1 can be any value between 1 and R_{crit}) reach parallelism with the vorticity vector, the a_3 axes start to rotate permanently within the VNS, and the R–ϕ plot starts to show a wide range of ϕ values at $R = R_1$ (Fig. 15b). At geologically realistic

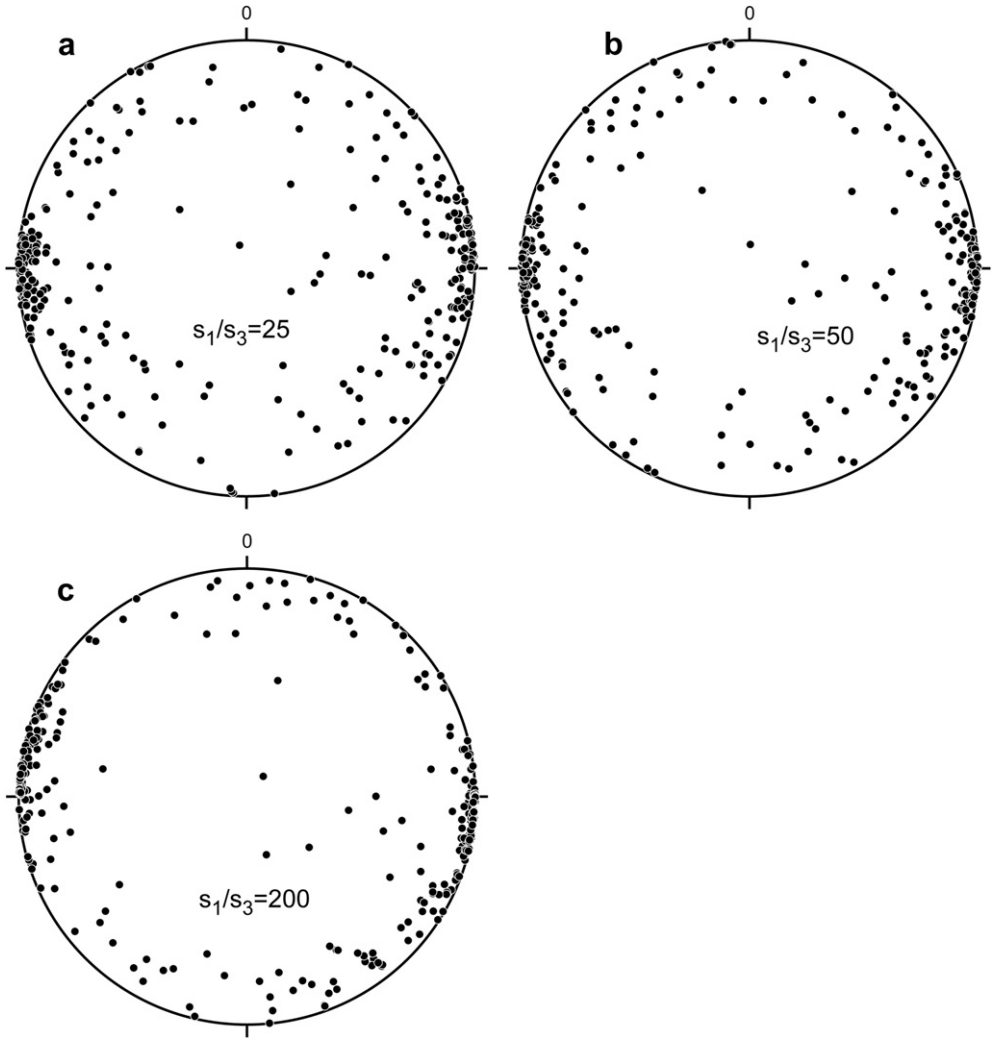

Fig. 17. Lower-hemisphere equal-area projections of the a_3 axes of 300 clasts at different finite strains in the S&M flow with W_k^s of 0.9. Clast initial orientations and shapes are the same as in Fig. 14. Note that a_3 axes quickly approach the normal to the shear zone boundary (a).

strains, few a_1 axes of clasts can reach parallelism with the vorticity vector (Fig. 14c), and type B clasts display ϕ values around zero defining a R_{cutoff} much smaller than R_{crit} (Fig. 9). Therefore large uncertainties exist in the ARC method (Figs. 6–10).

In plane-straining flows, clasts are either type A or type C. Similarly, at geologically realistic strains, very few a_2 axes of type A clasts can reach parallelism with the vorticity vector (Fig. 16), and a large uncertainty is introduced when treating them as stabilized clasts in the SC method. For the ARC method, R_{cutoff} cannot represent R_{crit} properly, which leads to a large uncertainty. In order for R_{cutoff} to represent R_{crit} properly, type C clasts are required to show a wide range of ϕ values at R close to R_{crit}. However, all type C clasts have a_1/a_3 ratio (r) less than R_{crit}, and only a few clasts in a population of clasts have r close to R_{crit}. Besides, R varies between 1 and r during deformation for a type C clast, and the chance is rare for a type C clast to show R equal or close to its r. Therefore, in plane-straining flows, type C clasts cannot show a wide range of ϕ values at R close to R_{crit}, and R_{cutoff} is generally less than R_{crit}. The ARC method can underestimate the vorticity number.

For the backward rotating clast (BRC) method, additional uncertainties can be introduced due to the difficulty in identifying forward/backward rotating clasts in practice. Fig. 18 is an example showing the R–ϕ polar plot of the rotation path of a triaxial clast (5.82:5.33:1) in the S&M flow with W_k^s of 0.7. This clast rotates forward first for 30° along vorticity axis before it rotates backward. In the R–ϕ plot, the transition (point T in Fig. 18) between forward rotation and backward rotation is not on the hyperbola. The fact that a clast can reverse its rotation sense during deformation introduces a serious problem for identifying the rotation sense from their tails because an instantaneously backward rotating clast may have forward rotated and may still retain tails suggesting forward rotating. This kind of uncertainty can be large. Although it is possible in numerical modeling to determine if a specific clast is momentarily forward or backward rotating, it is generally impossible to do so for natural rigid clasts. Because of this kind of uncertainty, we do not compare our numerical modeling results with those from practical vorticity analysis using the BRC method.

As discussed above, the uncertainties in the estimated vorticity number using the vorticity analysis methods are consequences of 3D rotation behavior of clasts. Therefore, the uncertainties are truly intrinsic, and cannot be removed.

6. Conclusions

Rigid clast motion relevant for natural rock deformation is an intrinsically 3D problem. Current vorticity analysis methods are

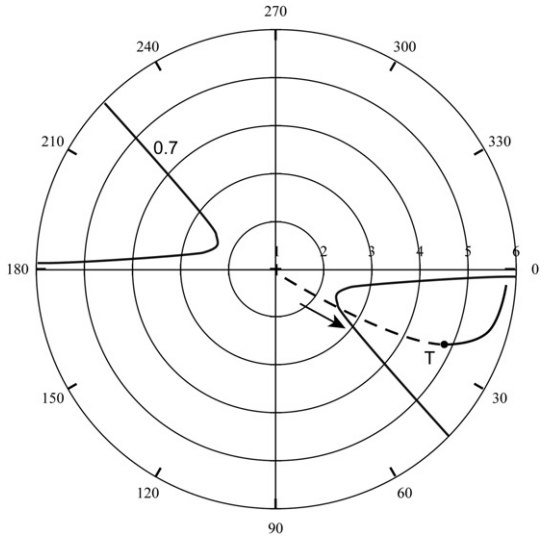

Fig. 18. $R-\phi$ plot of a single clast (a_1:a_2:a_3 = 5.82:5.33:1) rotation path in the S&M flow with W_k^s of 0.7. The hyperbola is constructed using Eqs. (7) and (8) for the W_k^s of 0.7. The initial orientation of the clast is a_1:10°, 143°, a_2: 45°, 052.5°, and a_3:44°, 160°. The clast rotates forward (dash line) first, and then rotates backward (solid line).

mainly based on the 2D theory of Ghosh and Ramberg (1976) which is inappropriate for clasts in natural rocks.

Even in flow fields that are homogeneous, steady state, and with monoclinic symmetries and assuming that clast rotation perfectly follows Jeffery's theory, the vorticity analysis methods using rigid clasts have intrinsic uncertainties so large that the results cannot be used to constrain the kinematics of natural shear zones. The large uncertainties associated with vorticity analysis using rigid clasts arise from 3D nature of rigid clast rotation.

Given the large intrinsic uncertainties in vorticity analysis using rigid clasts, the vorticity numbers between 0.5 and 0.85 reported in the literature using these methods could all have been produced in zones with close-to-simple-shearing flows.

Acknowledgements

We dedicate this paper to Paul Williams. DJ thanks Paul for mentorship and friendship. Paul's critical attitude to science has been a great inspiration. Being critical is not always welcome or well received. Paul used to say "It can be depressing to realize that some methods don't work and some problems in structural geology cannot be solved, but I would rather know what I cannot do or know, and work on what I can, than live in a fool's paradise". We have somehow written this paper for this special issue in Paul Williams' spirit. We thank P.-Y. Robin for his constructive review which helped us simplify some part of the paper. Reviewer Josef Ježek's comments have urged us to improve the presentation of the paper. Support from an NSERC Discovery Grant and a China National Science Foundation Grant (NSFC 40828001) to DJ is gratefully acknowledged.

References

Bailey, C., Eyster, E., 2003. General shear deformation in the Pinaleno Mountains metamorphic core complex, Arizona. Journal of Structural Geology 25 (11), 1883–1892.

Bjørnerud, M.G., Zhang, H., 1995. Flow mixing, object-matrix coherence, mantle growth and the development of porphyroclast tails. Journal of Structural Geology 17 (9), 1347–1350.

Bobyarchick, A.R., 1986. The eigenvalues of steady flow in Mohr space. Tectonophysics 122 (1–2), 35–51.

Carter, N.L., 1975. High-temperature flow of rocks. Reviews of Geophysics 13 (3), 344–349.

Carter, N.L., 1976. Steady state flow of rocks. Reviews of Geophysics 14 (3), 301–360.

Ceriani, S., Mancktelow, N.S., Pennacchioni, G., 2003. Analogue modelling of the influence of shape and particle/matrix interface lubrication on the rotational behaviour of rigid particles in simple shear. Journal of Structural Geology 25 (12), 2005–2021.

Fossen, H., Tikoff, B., 1993. The deformation matrix for simultaneous simple shearing, pure shearing, and volume change, and its application to transpression/transtension tectonics. Journal of Structural Geology 15 (3–5), 413–422.

Frassi, C., Carosi, R., Montomoli, C., Law, R.D., 2009. Kinematics and vorticity of flow associated with post-collisional oblique transpression in the Variscan Inner Zone of northern Sardinia (Italy). Journal of Structural Geology 31 (12), 1458–1471.

Freeman, B., 1985. The motion of rigid ellipsoidal particles in slow flows. Tectonophysics 113 (1–2), 163–183.

Gay, N.C., 1968. The motion of rigid particles embedded in a viscous fluid during pure shear deformation of the fluid. Tectonophysics 5 (2), 81–88.

Ghosh, S., Ramberg, H., 1976. Reorientation of inclusions by combination of pure shear and simple shear. Tectonophysics 34 (1–2), 1–70.

Gleason, G.C., Tullis, J., 1995. A flow law for dislocation creep of quartz aggregates determined with the molten salt cell. Tectonophysics 247 (1–4), 1–23.

Grasemann, B., Fritz, H., Vannay, J.C., 1999. Quantitative kinematic flow analysis from the Main Central Thrust Zone (NW-Himalaya, India): implications for a decelerating strain path and the extrusion of orogenic wedges. Journal of Structural Geology 21 (7), 837–853.

Grujic, D., Casey, M., Davidson, C., Hollister, L.S., Kündig, R., Pavlis, T., Schmid, S., 1996. Ductile extrusion of the Higher Himalayan Crystalline in Bhutan: evidence from quartz microfabrics. Tectonophysics 260 (1–3), 21–43.

Hobbs, B.E., Means, W.D., Williams, P.F., 1976. An Outline of Structural Geology. Wiley, New York.

Ildefonse, B., Mancktelow, N.S., 1993. Deformation around rigid particles: the influence of slip at the particle/matrix interface. Tectonophysics 221 (3–4), 345–359.

Ildefonse, B., Launeau, P., Bouchez, J.L., Fernandez, A., 1992a. Effect of mechanical interactions on the development of shape preferred orientations: a two-dimensional experimental approach. Journal of Structural Geology 14 (1), 73–83.

Ildefonse, B., Sokoutis, D., Mancktelow, N.S., 1992b. Mechanical interactions between rigid particles in a deforming ductile matrix. Analogue experiments in simple shear flow. Journal of Structural Geology 14 (10), 1253–1266.

Ildefonse, B., Arbaret, L., Diot, H., 1997. Rigid particles in simple shear flow: is their preferred orientation periodic or steady-state? In: Bouchez, J.L., Hutton, D.H.W., Stephens, W.E. (Eds.), Granites: From Melt Segragation to Emplacement Fabrics. Kluwer, Dordrecht, pp. 177–185.

Jeffery, G.B., 1922. The motion of ellipsoidal particles immersed in a viscous fluid. Proceedings of the Royal Society of London A102, 161–179.

Jessup, M.J., Law, R.D., Searle, M.P., Hubbard, M.S., 2006. Structural evolution and vorticity of flow during extrusion and exhumation of the Greater Himalayan slab, Mount Everest Massif, Tibet/Nepal: implications for orogen-scale flow partitioning. In: Law, R.D. (Ed.), Channel Flow, Ductile Extrusion and Exhumation in Continental Collision Zones. Geological Society, London, Special Publications, vol. 268, pp. 379–413.

Jessup, M.J., Law, R.D., Frassi, C., 2007. The Rigid Grain Net (RGN): an alternative method for estimating mean kinematic vorticity number (Wm). Journal of Structural Geology 29 (3), 411–421.

Ježek, J., Melka, R., Schulmann, K., Venera, Z., 1994. The behaviour of rigid triaxial ellipsoidal particles in viscous flows-modeling of fabric evolution in a multiparticle system. Tectonophysics 229 (3–4), 165–180.

Ježek, J., Schulmann, K., Segeth, K., 1996. Fabric evolution of rigid inclusions during mixed coaxial and simple shear flows. Tectonophysics 257 (2–4), 203–221.

Jiang, D., 1994. Flow variation in layered rocks subjected to bulk flow of various kinematic vorticities: theory and geological implications. Journal of Structural Geology 16 (8), 1159–1172.

Jiang, D., 1999. Vorticity decomposition and its application to sectional flow characterization. Tectonophysics 301 (3), 243–260.

Jiang, D., 2007. Numerical modeling of the motion of rigid ellipsoidal objects in slow viscous flows: a new approach. Journal of Structural Geology 29 (2), 189–200.

Jiang, D., 2010. Flow and finite deformation of surface elements in three dimensional homogeneous progressive deformations. Tectonophysics 487 (1–4), 85–99.

Jiang, D., White, J.C., 1995. Kinematics of rock flow and the interpretation of geological structures, with particular reference to shear zones. Journal of Structural Geology 17 (9), 1249–1265.

Jiang, D., Williams, P.F., 1998. High-strain zones: a unified model. Journal of Structural Geology 20 (8), 1105–1120.

Jiang, D., Williams, P.F., 1999. A fundamental problem with the kinematic interpretation of geological structures. Journal of Structural Geology 21 (8–9), 933–937.

Johnson, S.E., Lenferink, H.J., Price, N.A., Marsh, J.H., Koons, P.O., West, D.P., Beane, R., 2009. Clast-based kinematic vorticity gauges: the effects of slip at matrix/clast interfaces. Journal of Structural Geology 31 (11), 1322–1339.

Kirby, S.H., 1983. Rheology of the lithosphere. Reviews of Geophysics 21 (6), 1458–1487.

Klepeis, K.A., Daczko, N.R., Clarke, G.L., 1999. Kinematic vorticity and tectonic significance of superposed mylonites in a major lower crustal shear zone,

northern Fiordland, New Zealand. Journal of Structural Geology 21 (10), 1385–1405.
Kuiper, Y.D., Jiang, D., 2010. Kinematics of deformation constructed from deformed planar and linear elements: the method and its application. Tectonophysics 492 (1–4), 175–191.
Kurz, G.A., Northrup, C.J., 2008. Structural analysis of mylonitic rocks in the Cougar Creek Complex, Orogon-Idaho using the porphyroclast hyperbolic distribution method, and potential use of SC'-type extensional shear bands as quantitative vorticity indicators. Journal of Structural Geology 30 (8), 1005–1012.
Langille, J., Lee, J., Hacker, B., Seward, G., 2010. Middle crustal ductile deformation patterns in southern Tibet: insights from vorticity studies in Mabja Dome. Journal of Structural Geology 32 (1), 70–85.
Law, R.D., Searle, M.P., Simpson, R.L., 2004. Strain, deformation temperatures and vorticity of flow at the top of the Greater Himalayan Slab, Everest Massif, Tibet. Journal of the Geological Society, London 161, 305–320.
Lin, S., Jiang, D., Williams, P.F., 1998. Transpression (or transtension) zones of triclinic symmetry: natural example and theoretical modeling. In: Holdsworth, R.E., Strachan, R.A., Dewey, J.F. (Eds.), Continental Transpressional and Transtensioanl Tectonics. Geological Society, London, Special Publications, vol. 135, pp. 41–57.
Lister, G., Williams, P.F., 1983. The partitioning of deformation in flowing rock masses. Tectonophysics 92 (1–3), 1–33.
Liu, R., 2009. Deformation of the Clast-matrix System and its Application to the Microstructural analysis of mylonites. Unpublished M.Sc. Thesis, the University of Western Ontario.
Mancktelow, N.S., Arbaret, L., Pennacchioni, G., 2002. Experimental observations on the effect of interface slip on rotation and stabilisation of rigid particles in simple shear and a comparison with natural mylonites. Journal of Structural Geology 24 (3), 567–585.
Mandal, N., Kumar Samanta, S., Bhattacharyya, G., Chakraborty, C., 2005. Rotation behaviour of rigid inclusions in multiple association: insights from experimental and theoretical models. Journal of Structural Geology 27 (4), 679–692.
Marques, F.O., Bose, S., 2004. Influence of a permanent low-friction boundary on rotation and flow in rigid inclusion/viscous matrix systems from an analogue perspective. Tectonophysics 382 (3–4), 229–245.
Marques, F.G., Cobbold, P.R., 1995. Development of highly non-cylindrical folds around rigid ellipsoidal inclusions in bulk simple shear regimes: natural examples and experimental modelling. Journal of Structural Geology 17 (4), 589–602.
Marques, F.O., Coelho, S., 2001. Rotation of rigid elliptical cylinders in viscous simple shear flow: analogue experiments. Journal of Structural Geology 23 (4), 609–617.
Marques, F.O., Schmid, D.W., Anderson, T.B., 2007. Applications of inclusion behaviour models to a major shear zone system: the Nordfjore-Sogen Detachment zone in western Norway. Journal of Structural Geology 29 (10), 1622–1631.
Masuda, T., Michibayashi, K., Ohata, H., 1995. Shape preferred orientation of rigid particles in a viscous matrix; reevaluation to determine parameters of ductile deformation. Journal of Structural Geology 17 (1), 115–129.
Means, W.D., 1990. Kinematics, stress, deformation and material behavior. Journal of Structural Geology 12 (8), 953–971.
Means, W.D., Hobbs, B.E., Lister, G.S., Williams, P.F., 1980. Vorticity and non-coaxiality in progressive deformation. Journal of Structural Geology 2 (3), 371–378.
Mitra, G., 1978. Ductile deformation zones and mylonites; the mechanical processes involved in the deformation of crystalline basement rocks. American Journal of Science 278 (8), 1057–1084.
Mulchrone, K.F., 2007. An analytical solution in 2D for the motion of rigid elliptical particles with a slipping interface under a general deformation. Journal of Structural Geology 29 (6), 950–960.
Passchier, C.W., 1986. Flow in natural shear zones-the consequences of spinning flow regimes. Earth and Planetary Science Letters 77 (1), 70–80.
Passchier, C.W., 1987. Stable positions of rigid objects in non-coaxial flow: a study in vorticity analysis. Journal of Structural Geology 9 (5–6), 679–690.
Passchier, C.W., 1990. A Mohr circle construction to plot the stretch history of material lines. Journal of Structural Geology 12 (4), 513–515.
Passchier, C.W., 1997. The fabric attractor. Journal of Structural Geology 19 (1), 113–127.
Passchier, C.W., 1998. Monoclinic model shear zones. Journal of Structural Geology 20 (8), 1121–1137.
Passchier, C.W., Urai, J.L., 1988. Vorticity and strain analysis using Mohr diagrams. Journal of Structural Geology 10 (7), 755–763.
Pennacchioni, G., Fasolo, L., Cecchi, M.M., Salasnich, L., 2000. Finite-element modelling of simple shear flow in Newtonian and non-Newtonian fluids around a circular rigid particle. Journal of Structural Geology 22 (5), 683–692.
Pili, É., Ricard, Y., Lardeaux, J.M., Sheppard, S.M.F., 1997. Lithospheric shear zones and mantle-crust connections. Tectonophysics 280 (1–2), 15–29.
Ramberg, H., 1975a. Particle paths, displacement and progressive strain applicable to rocks. Tectonophysics 28 (1–2), 1–37.
Ramberg, H., 1975b. Superposition of homogeneous strain and progressive deformation in rocks. Bulletin of the Geological Institute of Uppsala, N.S 6, 35–67.
Ramsay, J., Graham, R., 1970. Strain variation in shear belts. Canadian Journal of Earth Sciences 7 (3), 786–813.
Ramsay, J.G., 1980. Shear zone geometry: a review. Journal of Structural Geology 2 (1–2), 83–99.
Ratschbacher, L., Wenk, H., Sintubin, M., 1991. Calcite textures-examples from nappes with strain-path partitioning. Journal of Structural Geology 13 (4), 369–384.
Regenauer-Lieb, K., Yuen, D.A., 2003. Modeling shear zones in geological and planetary sciences: solid- and fluid-thermal–mechanical approaches. Earth-Science Reviews 63 (3–4), 295–349.
Robin, P.F., Cruden, A.R., 1994. Strain and vorticity patterns in ideally ductile transpression zones. Journal of Structural Geology 16 (4), 447–466.
Sanderson, D.J., Marchini, W.R.D., 1984. Transpression. Journal of Structural Geology 6 (5), 449–458.
Sarkarinejad, K., Azizi, A., 2008. Slip partitioning and inclined dextral transpression along the Zagros Thrust System, Iran. Journal of Structural Geology 30 (1), 116–136.
Sarkarinejad, K., Godin, L., Faghih, A., 2009. Kinematic vorticity flow analysis and $^{40}Ar/^{39}Ar$ geochronology related to inclined extrusion of the HP–LT metamorphic rocks along the Zagros accretionary prism, Iran. Journal of Structural Geology 31 (7), 691–706.
Savage, M.K., 1999. Seismic anisotropy and mantle deformation: what have we learned from shear wave. Reviews of Geophysics 37 (1), 65–106.
Schmid, D.W., Podladchikov, Y.Y., 2004. Are isolated stable rigid clasts in shear zones equivalent to voids? Tectonophysics 384 (1–4), 233–242.
Schmid, D.W., Podladchikov, Y.Y., 2005. Mantled porphyroclast gauges. Journal of Structural Geology 27 (3), 571–585.
Short, H.A., Johnson, S.E., 2006. Estimation of vorticity from fibrous calcite veins, central Maine, USA. Journal of Structural Geology 28 (7), 1167–1182.
Simpson, C., De Paor, D.G., 1993. Strain and kinematic analysis in general shear zones. Journal of Structural Geology 15 (1), 1–20.
Simpson, C., De Paor, D.G., 1997. Practical analysis of general shear zones using the porphyroclast hyperbolic distribution method: an example from the Scandinavian Cavedonides. In: Sengputta, S. (Ed.), Evolution of Geological Structues in Micr- to Macro-Scales. Chapman & Hall, London, pp. 169–184.
Sullivan, W.A., 2008. Significance of transport-parallel strain variations in part of the Raft River shear zone, Raft River Mountains, Utah, USA. Journal of Structural Geology 30 (2), 138–158.
Tchalenko, J.S., 1970. Similarities between shear zones of different Magnitudes. Geological Society of America Bulletin 81 (6), 1625–1640.
Thigpen, R.J., Law, R.D., Lloyd, G.E., Brown, S.J., 2010. Deformation temperatures, vorticity of flow, and strain in the Moine thrust zone and Moine nappe: reassessing the tectonic evolution of the Scandian foreland-hinterland transition zone. Journal of Structural Geology 32 (7), 920–940.
Tikoff, B., Fossen, H., 1995. The limitations of three-dimensional kinematic vorticity analysis. Journal of Structural Geology 17 (12), 1771–1784.
Truesdell, C.A., 1953. Two measures of vorticity. Journal of Rational Mechanics Analysis 2, 173–217.
Truesdell, C.A., 1954. The Kinematics of Vorticity. Indiana University Press, Bloomington.
Truesdell, C.A., 1991. A First Course in Rational Continuum Mechanics. Academic Press.
Tullis, J.A., 1979. High temperature deformation of rocks and minerals. Reviews of Geophysics 17 (6), 1137–1154.
Vauchez, A., Tommasi, A., 2003. Wrench faults down to the asthenosphere: geological and geophysical evidence and thermo-mechanical effects. In: Storti, F. (Ed.), Intraplate Strike-slip Deformation Belts. Geological Society, London, Special Publications, vol. 210, pp. 15–34.
Vissers, R.L.M., 1989. Asymmetric quartz *c*-axis fabrics and flow vorticity: a study using rotated garnets. Journal of Structural Geology 11 (3), 231–244.
Wallis, S.R., 1992. Vorticity analysis in a metachert from the Sanbagawa belt, SW Japan. Journal of Structural Geology 14 (3), 271–280.
Wallis, S.R., 1995. Vorticity analysis and recognition of ductile extension in the Sanbagawa belt, SW Japan. Journal of Structural Geology 17 (8), 1077–1093.
Wallis, S.R., Platt, J.P., Knott, S.D., 1993. Recognition of syn-convergence extension in accretionary wedges with examples from the Calabrian Arc and the Eastern Alps. American Journal of Science 293 (5), 463–494.
Wang, X., Zheng, Y., Wang, T., 2007. Strain and shear types of the Louzidian ductile shear zone in southern Chifeng, Inner Mongolia, China. Science in China, Series D: Earth Sciences 50 (4), 487–495.
Wenk, H.R., Takeschita, T., Bechler, E., Erskine, B.G., Matthies, S., 1987. Pure shear and simple shear calcite textures: comparison of experimental, theoretical and natural data. Journal of Structural Geology 9 (5–6), 731–745.
Williams, P.F., Jiang, D., 2005. An investigation of lower crustal deformation: evidence for channel flow and its implications for tectonics and structural studies. Journal of Structural Geology 27 (8), 1486–1504.
Xypolias, P., Doutsos, T., 2000. Kinematics of rock flow in a crustal-scale shear zone: implication for the orogenic evolution of the southwestern Hellenides. Geological Magazine 137 (1), 81–96.
Xypolias, P., Koukouvelas, I.K., 2001. Kinematic vorticity and strain rate patterns associated with ductile extrusion in the Chelmos Shear Zone (External Hellenides, Greece). Tectonophysics 338 (1), 59–77.
Zhang, B., Zhang, J., Zhong, D., Guo, L., 2009. Strain and kinematic vorticity analysis: an indicator for sinistral transpressional strain-partitioning along the Lancangjiang shear zone, western Yunnan, China. Science in China Series D: Earth Sciences 52 (5), 602–618.